ESD-TR-91-244

Technical Report
946

Optimal Three-Dimensional Matched Filter Processing for Detection of Point-Like Moving Objects in Clutter

J.N. Sanders

30 September 1992

Lincoln Laboratory
MASSACHUSETTS INSTITUTE OF TECHNOLOGY
LEXINGTON, MASSACHUSETTS

Prepared for the Department of the Air Force under Contract F19628-90-C-0002.

This report is based on studies performed at Lincoln Laboratory, a center for research operated by Massachusetts Institute of Technology. The work was sponsored by the Strategic Defense Initiative Organization under Air Force Contract F19628-90-C-0002.

The ESD Public Affairs Office has reviewed this report, and it is releasable to the National Technical Information Service, where it will be available to the general public, including foreign nationals.

This technical report has been reviewed and is approved for publication.

FOR THE COMMANDER

Gary Tutungian
Administrative Contracting Officer
Directorate of Contracted Support Management

MASSACHUSETTS INSTITUTE OF TECHNOLOGY
LINCOLN LABORATORY

OPTIMAL THREE-DIMENSIONAL MATCHED FILTER PROCESSING FOR DETECTION OF POINT-LIKE MOVING OBJECTS IN CLUTTER

J.N. SANDERS
Group 96

TECHNICAL REPORT 946

30 SEPTEMBER 1992

LEXINGTON **MASSACHUSETTS**

ABSTRACT

A simple model of a time sequence of star images containing a moving point object (satellite) is developed. Optimal signal enhancement and detection processing theory is applied to this model and a three-dimensional Fourier matched filter implementation is derived to compute clutter-to-noise ratio (CNR) suppression, signal-to-noise ratio (SNR) enhancement, and probability of detection (P_d) and false alarm (P_{fa}) rate estimates as a function of input single pixel SNR. Using this theory allows one to compute the Fourier domain matched filters directly, thereby eliminating the enormous storage cost associated with large banks of three-dimensional matched filters. The model and theory are tested using computer-generated simulated data sets having known noise and clutter characteristics. The theory is then applied to real data sets collected using a Lincoln Laboratory CCD camera. Initial results indicate good agreement with matched filter theory. Detection of objects with an initial single pixel SNR ≈ 1 is demonstrated.

ACKNOWLEDGMENTS

Tony Filip provided extensive and valuable feedback throughout all phases of the development of this report. Peter Tennyson provided insights into the problems of satellite detection, the limitations of existing approaches, the differences between theory and reality, and the star map clutter suppression demonstration and data. Stephen Pohlig explained the maximum likelihood normalizer and beta distribution.

TABLE OF CONTENTS

LIST OF ILLUSTRATIONS

LIST OF ILLUSTRATIONS (Continued)

LIST OF TABLES

1. INTRODUCTION

Satellite detection from ground- and space-based optical sensors entails acquiring a sequence of two-dimensional intensity images, thereby forming a three-dimensional image volume with two spatial coordinates and one time coordinate. Lincoln Laboratory uses a camera containing a CCD chip with 420 × 420 pixels in the focal plane. Versions of the chip are available that can be mounted flush with each other to give 840 × 840 or more pixels per frame. Most of the existing data sets used in this study consist of 16 consecutive frames of data, although many more could easily be collected. Integration times per frame are typically 0.2 to 5 s. The result of this data collection process is an image volume of $N_x \times N_y \times N_t$ pixels, where N_x and N_y are the number of pixels in the two-dimensional CCD focal plane array, and N_t is the number of frames of data.

Images collected in this process typically contain noise, stars, and possibly one or more satellites. The stars and the satellites are imaged as unresolved point sources. The most common method of data collection is sidereal track mode, wherein the telescope tracks the stars, which remain fixed on the focal plane. In the sidereal case a satellite moves across the detector, forming a steak. Another data collection method is the ephemeris track mode, which requires an estimate of the satellite orbit. With this method the telescope tracks the satellite, which remains fixed on the focal plane, while the stars form streaks on the detector. To detect a satellite a differentiation must be made between the stars (moving at one velocity on the focal plane) and a satellite (moving at a different velocity). Furthermore, in the case of a faint satellite the single pixel signal-to-noise ratio (SNR) may be considerably less than one, making it essentially undetectable to the unaided observer. Thus there are two tasks to be performed: clutter (star) suppression and signal enhancement, shown schematically in Figure 1.

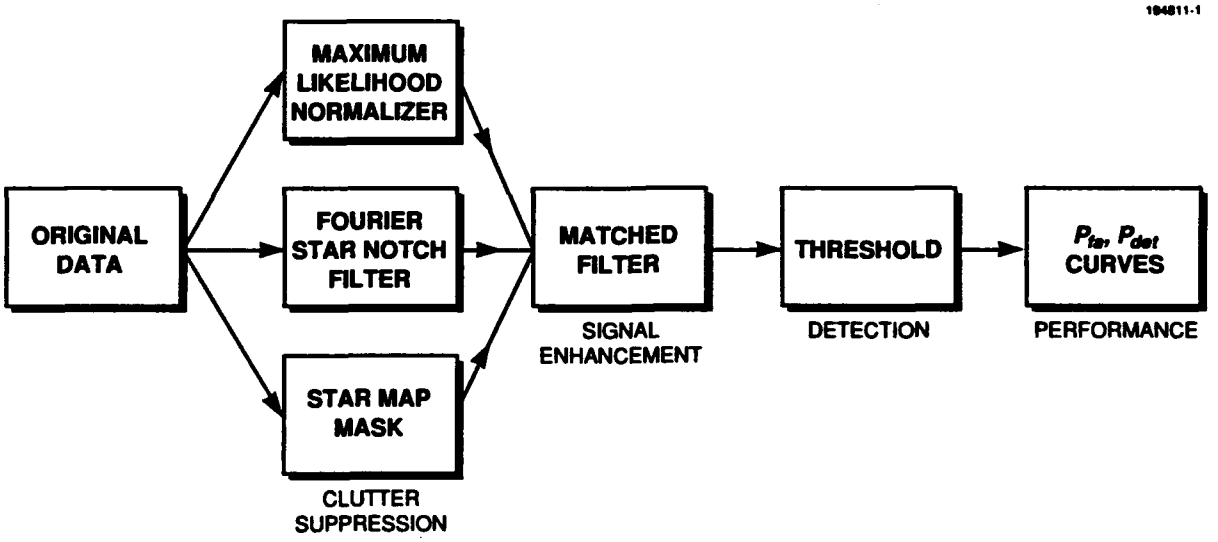

Figure 1. Matched filter detection processing chain.

The purpose of this report is to develop and test a model of the image sets used for satellite detection and a corresponding detection theory. Insights gained from this work are used to evaluate current state-of-the-art signal processing algorithms. Probability of detection (P_d) and of false alarm (P_{fa}) curves are determined for the theory as a function of single pixel SNR. Theoretically predicted SNR enhancement values can then be compared with results from real data sets to assess the validity of the current model. The discussion begins with matched filter theory as the optimal linear technique to determine the presence and location of a known signal in a background of stationary noise [1]. If the input signal is sufficiently well behaved (stationary Gaussian statistics), the linear matched filter represents *the* optimal processing at any order. Detection can be performed using either a correlation function in the space-time volume or the mathematically equivalent matched filter approach in the Fourier transform volume [2]. Reed [3] has extended the common one-dimensional filter used in radar applications and the two-dimensional filter used for images to a three-dimensional time sequence of images. Reed [4] and Porat [5] have each discussed the application of matched filters to the three-dimensional point object detection problem. The nature of the Fourier volume for this application and the form of the matched filter will be explored. Next is the question of detectability: What is the relation between satellite brightness, noise level, observation time, and detection capability?

The theory is initially developed for a continuous case (both spatial and temporal) for analytic simplicity and clarity. (A discrete formulation is presented in the appendix, and data representing a discretely sampled image volume is generated and used to verify the theory.) To perform the signal enhancement step, one must first perform clutter suppression. Thus three methods are explored: a frequency slice based on the matched filter theory, a maximum likelihood normalizer, and a star map technique that introduces additional information to suppress the clutter. Results for two- and three-dimensional data sets, both computer generated and real, are presented. These data sets verify the algorithm and allow a comparison of the model with real-life data, which introduce Poisson noise, mount jitter, and effects due to the finite size of the CCD cells.

2. THEORY

2.1 THE SPATIAL DOMAIN MODEL

To understand the image data and generate a sensitive detection algorithm, it is useful to form an analytical model of the image data. Scribner has developed a model for the entire image chain, from object radiance through the imaging hardware to the final electronic image [6]. This model includes factors for the optics point spread function (PSF) and the effects of discrete sampling. A simpler approach is taken here with the focus on the image set. The signal intensity at any given pixel will be the sum of a white noise contribution (I_η) and possible contributions from stars (I_ξ) and/or satellites (I_s), that is, $I(x,t) = I_\eta(x,t) + I_\xi(x,t) + I_s(x,t)$.

The discrete image volume is composed of $N_x \times N_y \times N_t$ pixels, each having volume $v_s = p_x p_y p_t$. The total image volume is then $V_s = L_x L_y T$, where $L_x = p_x N_x$, $L_y = p_y N_y$, and $T = p_t N_t$ but for convenience is denoted by (L,T).

Both the stars and satellites may be described as diffraction-limited Gaussian spots falling on the focal plane of a telescope with the same Gaussian width parameter σ. For now the Poisson nature of the photon statistics is ignored and constant irradiance is assumed. Stars are described by the intensity distribution

$$I_\xi(\bar{x},t) = \sum_i A_i e^{-\frac{(\bar{x}-\bar{x}_i(t))^2}{2\sigma^2}} \quad , \tag{1}$$

where the sum is over all stars and they are moving at the same velocity $\bar{v}_\xi : \bar{x}_i(t) = \bar{x}_i + \bar{v}_\xi t$. A satellite in the image is described by a similar distribution,

$$I_s(\bar{x},t) = A_s(t) e^{-\frac{\left(\bar{x}-\bar{x}_s(t)\right)^2}{2\sigma^2}} \quad . \tag{2}$$

The satellite is moving at a different velocity, $\bar{v}_s : \bar{x}_s(t) = \bar{x}_s + \bar{v}_s t$. The velocities are two-dimensional focal plane velocities (e.g., millimeters per second). In discrete focal plane coordinates v_s could be written (in one dimension) as $v_s = p_x v_f / p_t$, where v_f is now in pixels/frame. The time dependence of $A_s(t)$ represents tumbling or rotating objects as well as changes in the sun, satellite, or observer angle. For this study the time independent form $A_s(t) = A_s$ is used. The units of A_s and the A_i are irradiance:

$$A_{i,s}[=]\frac{\text{energy}}{\text{area} \bullet \text{time}}[=]\frac{\text{power}}{\text{area}} \quad .$$

The rest of this section discusses only the signal due to a satellite; however, because the PSFs are identical, the stars behave identically.

The energy deposited per frame time (p_t) by a satellite is

$$E_s(p_t) = \int_0^{p_t} \int_{-\infty}^{+\infty} I_s(\bar{x},t)\,d\bar{x}\,dt$$

$$= \int_0^{p_t} \int_{-\infty}^{+\infty} A_s e^{-\left(\bar{x}-\bar{x}_s(t)\right)^2/\left(2\sigma^2\right)}\,d\bar{x}\,dt$$

$$E_s(p_t) = 2\pi\sigma^2 A_s p_t \quad . \tag{3}$$

While the focal plane is obviously finite, it is sufficiently large compared with the Gaussian PSF to use the infinite integrals for all streaks except those that actually leave the focal plane. This energy may be confined to a single pixel or spread among several, depending on $\bar{v}_s$.

A useful reality check after the transforms are made is Parseval's Theorem $P = \int f^2(x)dx = \int g^2(\omega)d\omega$:

$$P = \int_0^{T} \int_{-\infty}^{+\infty} I_s^2(\bar{x},t)\,d\bar{x}\,dt = \pi\sigma^2 A_s^2 T [=] \frac{\text{energy}^2}{\text{area} \bullet \text{time}} \quad .$$

An average energy deposited per area along the streak in the focal plane is easily computed by

$$e_s = \frac{\text{energy / frame}}{\text{streak length} \bullet \text{streak width}} \quad .$$

If the Gaussian spot size is defined as 2σ, the streak length may be written as $2\sigma + |\bar{v}_s| p_t$, giving

$$e_s = \frac{E_s(p_t)}{\left(2\sigma + |\bar{v}_s| p_t\right) \bullet 2\sigma}$$

$$e_s = \frac{\pi\sigma A_s p_t}{2\sigma + |\bar{v}_s| p_t} \quad .$$

However, to compute a single pixel SNR an energy deposited per pixel must be computed. In general, even with an infinitesimal point distribution, a single value is not observed because a point moving at an angle with respect to the two spatial axes moves diagonally through the pixel grid, thereby cutting through corners of some pixels and depositing more energy in some than in others. The situation is even more complicated when using a finite PSF.

If the physical dimensions of the CCD pixels are $p_x = p_y$, and the spot area ($2\pi\sigma^2$) is much less than the pixel area, then for a streak parallel to the x-axis and centered on the row of pixels, two general cases can be distinguished. If the velocity is sufficiently slow that the object *can* be entirely contained within

a single pixel, then the energy per pixel is the energy per frame. Note however, that as long as $\bar{v} \neq 0$, there are some frames where the energy is distributed between two pixels. If the velocity times integration time is greater than a single pixel, then the energy per pixel is the energy per frame times the ratio of a pixel length to the streak length. Thus the energy per pixel is

$$e_s = \begin{cases} E_s(p_t) & |\bar{v}_s| p_t < p_x \\ E_s(p_t) \dfrac{p_x}{|\bar{v}_s| p_t} & |\bar{v}_s| p_t > p_x \end{cases} , \tag{4}$$

which will be used as a general approximation to the single pixel SNR. It is also useful to determine the total number of pixels contained in such a streak:

$$\Omega = \frac{|\bar{v}_s| p_t N_t}{p_x} = \frac{|\bar{v}_s| T}{p_x} . \tag{5}$$

Equation (5) undercounts the true number of pixels in a streak because of the discrete nature of the frames. A better formula would compute $|\bar{v}_s| \rho_r / \rho_x$, round up to the next highest integer, and multiply by N_t. For this work the simpler formulation is sufficient.

Noise in the image volume may be described by a white (in both space and time) Poisson dark current, which may be written as a constant component $\bar{\eta}$ plus a zero mean noise component of amplitude ε: $\eta = \bar{\eta} \pm \varepsilon$, where ε is drawn from a normal distribution characterized by standard deviation $\rho = \sqrt{\eta}$. For the fluctuation portion the autocorrelation function is written

$$R_\eta(\bar{\chi}, \tau) = \left\langle I_\eta(\bar{x}, t) \bullet I_\eta(\bar{x} - \bar{\chi}, t - \tau) \right\rangle = \rho^2 \delta(\bar{\chi}, \tau) , \tag{6}$$

and the expectation value in any volume element (pixel) V_s is written

$$\left\langle I_\eta(\bar{x}, t) \right\rangle = \bar{\eta} V_s = \eta_p$$

$$\sqrt{\left\langle \varepsilon^2(x,t) \right\rangle} = \pm \rho \sqrt{V_s} = \pm \sqrt{\eta V_s} = \pm \rho_p ,$$

where ρ_p is the observed standard deviation of the pixels. The total noise energy is then $E_\eta = \bar{\eta} V_s$, but the Parseval "energy" is $P = \bar{\eta}^2 V_s + \rho^2 V_s = (\bar{\eta}^2 + \bar{\eta}) V_s$.

Other phenomena that are observed in actual images but ignored in this model include

- Fixed pattern noise
- Saturation effects
- Time varying effects resulting from cloud motion
- Atmospheric and mount jitter

- Radiation effects (gamma events)
- Target signature
- Photon Poisson statistics of stars and targets.

2.2 DETECTION THEORY

Several optimal processing algorithms are available, depending on whether the objective is to

- Determine if a signal of known signature is present in a random noise background, and if it is, to locate it (linear matched filter)
- Determine if a random signal, having known power spectra, is present in a random noise background (stochastic matched filter)
- Recover, as well as possible, the signature of an unknown signal in a random noise background (Wiener or least mean square filter).

Each task is slightly different and requires a different mathematical approach [7,8].

For a simple, one-dimensional, time varying signal $s(t)$, its Fourier transform (amplitude spectrum) can be written as $S(\omega) = \mathcal{F}(s(t))$. An additive noise source $\eta(t)$ with autocorrelation function $R(\tau) = \langle \eta(t)\eta(t-\tau) \rangle$ has a Fourier power spectrum $|N(\omega)|^2 = \mathcal{F}(R(\tau))$. In this case the optimal detection matched filter is [1]

$$H(\omega) = \frac{S^*(\omega) e^{i\omega t_o}}{|N(\omega)|^2} \quad ,$$

where $S^*(\omega)$ is the complex conjugate of $S(\omega)$. The phase factor allows the output detection peak to be shifted from the true object location τ to $\tau + t_o$. In practice t_o is usually set to zero. The filtering operation is described $s'(t) = \mathcal{F}^{-1}(S(\omega)H(\omega))$. Detections now correspond to peaks in the output signal $s'(t)$. A threshold can be set at a given level above the background noise level to yield a desired P_d or P_{fa}. If the signal is a rectangle function, then filtering with the above matched filter gives a triangle function output: an optimal detection but bearing little resemblance to the input signal. In three dimensions this detection becomes

$$H(\bar{k},\omega) = \frac{S^*(\bar{k},\omega)}{|N(\bar{k},\omega)|^2} e^{i(\bar{k}\cdot\bar{x}_o + \omega t_o)} \tag{7}$$

Because the matched filter is designed to optimize the output SNR, the well-known result of using a matched filter in the presence of white noise ($N(\bar{k},\omega) = N$) is that the final SNR depends only on the total signal energy and not its spatial distribution. For the current situation, when the signal increases linearly with observation time and the noise increases as the square root, the matched filter is expected

to increase the SNR by the square root of the number of frames of data collected. The signal enhancement process is depicted geometrically in Figure 2.

Referring to Figure 2(a), for the objects that are present for the entire observation time, the signal peaks in a predetermined plane. In this case one need only back transform the single desired temporal plane to perform the detection. This procedure is accomplished following the filtering operation by performing the inverse temporal transform only for $t = t_o$; however, if one desires to perform further operations in addition to basic detection, such as position estimation, the use of the full three-dimensional result may be required.

The result of performing a two-dimensional back transform is a single x-y frame of data having a correlation spike at the $t = t_o$ location of the target. The shape of this spike is the autocorrelation of a rectangle the length of a single frame streak, whereas the full three-dimensional form produces the autocorrelation of the entire streak. Two things are accomplished: first, the size of the back transform that must be applied for each filter is reduced, and second, by collapsing the broad triangle to the much narrower single frame correlation triangle, detection processing is simplified.

The matched filter operation in the Fourier volume corresponds to the correlation function in the space-time domain:

$$\mathcal{F}^{-1}\left(F(\omega)G^*(\omega)\right) = \int_{-\infty}^{+\infty} f(\tau+t)g(\tau)d\tau \quad .$$

In fact, for the filter $H(\omega) = S^*(\omega)$, the matched filter is an autocorrelation function. The Fourier domain arbitrary phase factor is equivalent to the addition of a time delay t_o in the argument to the filter function.

In three dimensions the enhanced signal is

$$f(\bar{x},t) = \iiint_{+\infty}^{-\infty} g(\bar{\chi},\tau)h(\bar{\chi}+\bar{x},\tau+t-t_o)d\bar{\chi}d\tau \quad .$$

To illustrate, using a δ-function target moving at constant velocity $\bar{v}$ observed for the interval $0 < \tau < T$:

$$g(\bar{\chi},\tau) = I(\tau)\delta(\bar{\chi}-\bar{\chi}_0-\bar{v}\tau) \quad ,$$

and use the following relation,

$$\int_{-\infty}^{+\infty} \delta(\chi)\delta(x+\chi)d\chi = \delta(x) \quad ,$$

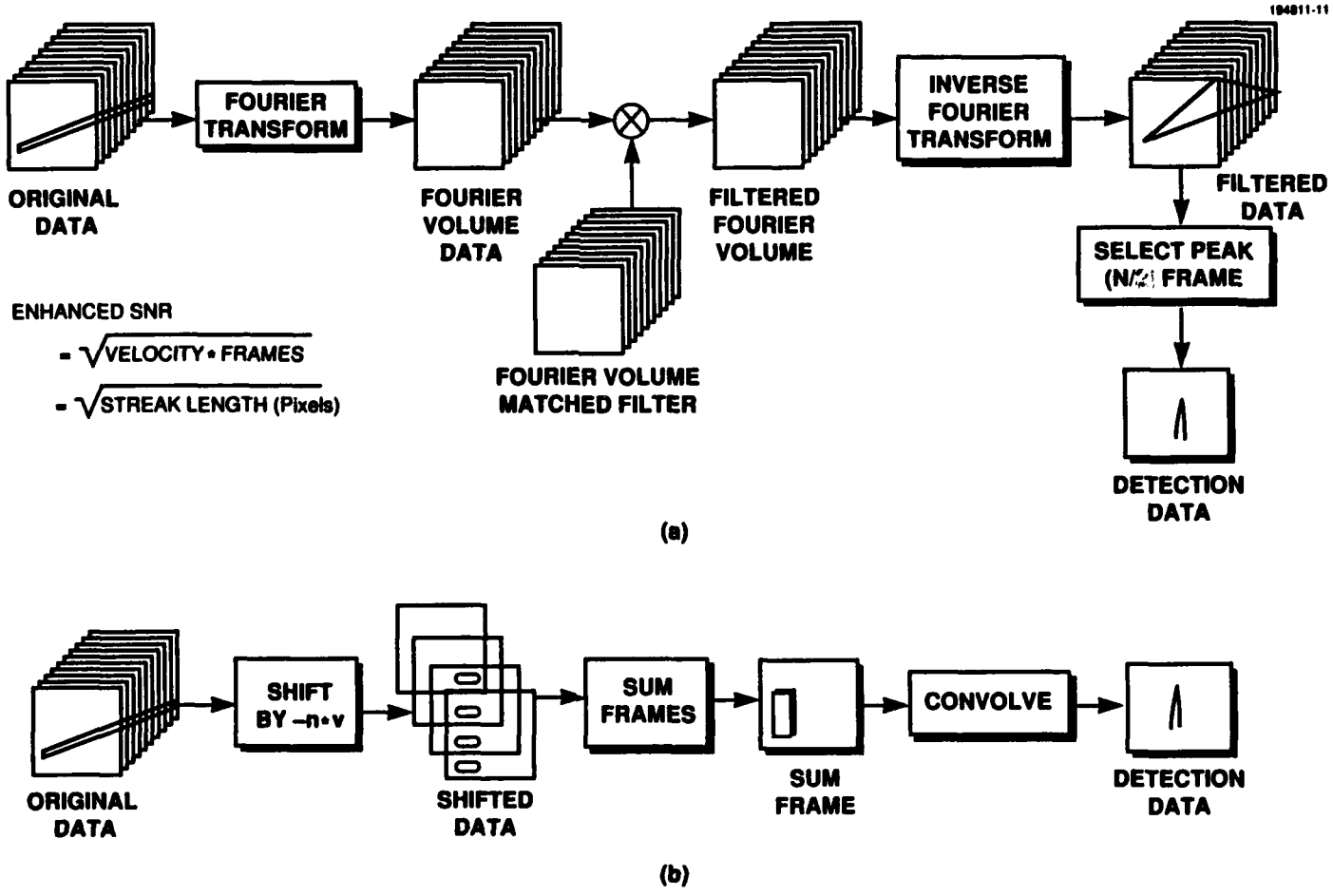

Figure 2. Signal enhancement techniques: (a) Fourier transform matched filter processing and (b) space-time convolution processing, "shift-and-add."

the correlation reduces to a one-dimensional integral:

$$f(\bar{x},t)=\int_{-\infty}^{+\infty} I(\tau)I(\tau+t-t_o)\delta(\bar{x}-\bar{x}_o-\bar{v}\tau)d\tau \quad . \tag{8}$$

The δ function serves to select the proper x position as a function of time. Because a priori knowledge of the target signature $I(\tau)$ is lacking, let the filter profile become a rectangle function of amplitude I_o. If the spatial dependence is temporarily dropped for simplicity, Equation (8) becomes:

$$f(t)=\begin{cases} \int_{t_o}^{t+T} I_o I(\tau)d\tau & -T+t_o<t<t_o \\ \int_{t}^{T+t_o} I_o I(\tau)d\tau & t_o<t<T+t_o \\ 0 & \text{otherwise} \end{cases} \quad . \tag{9}$$

This equation is a useful form for exploring the nature of the enhanced signal. In the case of a constant amplitude signal ($I(\tau) = I_o$), the result is a triangle of width $2T$ and amplitude I_o^2T centered at $t = t_o$:

$$f(t)=\begin{cases} I_o^2(t+T-t_o) & -T+t_o<t<t_o \\ I_o^2(t+T-t_o) & t_o<t<T+t_o \\ 0 & \text{otherwise} \end{cases} \quad .$$

If $I(t)$ remains strictly positive, the result will still be centered at $t = t_o$ but no longer symmetric. For a constant brightness target in the presence of noise, $I(t)$ can be replaced with $I_o + h(t)$, where $h(t)$ is a normally distributed random variable characterized by width r. The initial single point SNR is then simply $I_o/h(t)$ or on average I_o/r. The enhanced signal at $t = t_o$ is ${I_o}^2T + \sqrt{\Sigma_i(I_o\eta_i^2)} \approx I_o^2T + I_o\rho\sqrt{T}$, which represents an SNR increase of $\sqrt{T}$.

2.3 FOURIER VOLUME DEVELOPMENT

The extent of the Fourier volume is determined by the resolution in the image volume while the resolution in the Fourier volume is determined by the extent of the image volume:

$$V_F^{-1} = \frac{L_x L_y T}{(2\pi)^3} = \frac{V_s}{(2\pi)^3}$$

$$V_F^{-1} = \frac{P_x P_y P_t}{(2\pi)^3} = \frac{V_s}{(2\pi)^3}$$

For analytical purposes it is convenient to change the origin to $T/2$ so that integration is from $-T/2$ to $+T/2$ rather than 0 to T. The three-dimensional Fourier transform is:

$$G(\bar{k},\omega) = \mathcal{F}(I(\bar{x},t)) = \left[\frac{1}{\sqrt{2\pi}}\right]^3 \int_{-T/2}^{+T/2}\int_{-\infty}^{-\infty}\iint I(\bar{x},t)e^{-i\bar{k}\cdot\bar{x}-i\omega t}\,d\bar{x}\;dt$$

$$G(\bar{k},\omega) = \left[\frac{1}{\sqrt{2\pi}}\right]^3 \int_{-T/2}^{+T/2}\int_{-\infty}^{+\infty}\iint \left[I_\eta(\bar{x},t) + I_\xi(\bar{x},t) + I_s(\bar{x},t)\right]e^{-i\bar{k}\cdot\bar{x}-i\omega t}\,d\bar{x}\;dt$$

$$= G_\eta(\bar{k},\omega) + G_\xi(\bar{k},\omega) + G_s(\bar{k},\omega)$$

Using the current model for the detected image volume, the Fourier amplitude spectrum may now be computed. The Fourier spectrum for a satellite is

$$G_s(\bar{k},\omega) = \frac{1}{\sqrt{2\pi}^3}\int_{-T/2}^{+T/2}\int_{-\infty}^{+\infty}\iint A_s e^{-\frac{\left(\bar{x}-\bar{x}_s(t)\right)^2}{2\sigma^2}} e^{-i\bar{k}\bullet\bar{x}-i\omega t}\,d\bar{x}\,dt$$

$$= \frac{\sigma^2 A_s e^{-i\bar{k}\bullet\bar{x}_s} e^{-\frac{\sigma^2\bar{k}\bullet\bar{k}}{2}}}{\sqrt{2\pi}}\int_{-T/2}^{+T/2} e^{-i\left(\omega+\bar{k}\bullet\bar{v}_s\right)t}\,dt$$

$$G_s(\bar{k},\omega) = \frac{\sigma^2 A_s T e^{-i\bar{k}\bullet\bar{x}_s} e^{-\frac{\sigma^2\bar{k}\bullet\bar{k}}{2}}}{\sqrt{2\pi}}\,\mathrm{sinc}\left[\left(\omega+\bar{k}\bullet\bar{v}_s\right)\frac{T}{2}\right] \qquad (10)$$

Lacking knowledge of the expected target location, the matched filter will be the complex conjugate of the position-independent portion of Equation (10), which is strictly real. Hence, $H(\omega) = H^*(\omega)$.

$$H(\bar{k},\omega) = \frac{\sigma^2 A_s T e^{-\frac{\sigma^2 \bar{k}\bullet\bar{k}}{2}}}{\sqrt{2\pi}} \operatorname{sinc}\left[\left(\omega + \bar{k}\bullet\bar{v}_s\right)\frac{T}{2}\right] \quad . \tag{11}$$

An equivalent representation using the discrete Fourier transform is presented in the Appendix. At this point it is worth noting that the streak in the space-time domain represented the convolution of a Gaussian PSF with an infinitesimal line. Thus as expected, the previous expression is the Fourier transform of the Gaussian multiplied by the Fourier transform of the streak, according to the identity

$$\mathcal{F}\left\{g(\bar{x},t) * l(\bar{x},t)\right\} = \mathcal{F}\left\{G(\bar{k},\omega)\right\} \bullet \mathcal{F}\left\{L(\bar{k},\omega)\right\} \quad . \tag{12}$$

The Fourier power spectrum is

$$\left|G_s(\bar{k},\omega)\right|^2 = \frac{\sigma^4 A_s^2 T^2 e^{-\sigma^2 \bar{k}\bullet\bar{k}}}{2\pi} \operatorname{sinc}^2\left[\left(\bar{k}\bullet\bar{v}_s + \omega\right)\frac{T}{2}\right] \quad . \tag{13}$$

If $\sigma \to 0$ such that $\sigma^2 A_s \to B_s$, then

$$\left|G_s(\bar{k},\omega)\right|^2 = \frac{B_s^2 T^2}{2\pi} \operatorname{sinc}^2\left[\left(\bar{k}\bullet\bar{v}_s + \omega\right)\frac{T}{2}\right] \quad .$$

The signal is maximized in the $\bar{k}\bullet\bar{v}_s = -\omega$ plane:

$$\left|G_s\left(\bar{k}\bullet\bar{v}_s = -\omega\right)\right|^2 = \frac{B_s^2 T^2}{2\pi} = \frac{B_s^2 T}{\delta\omega} \quad ,$$

where the smallest resolvable gradation in the frequency domain, $\delta\omega = 2\pi/T$, has been used and is called the width of the plane. As observation time increases more signal is collected, while at the same time occupying a smaller volume in Fourier space. The preceding discussion demonstrates that the contribution due to the satellite is confined to a single plane, $\bar{k}\bullet\bar{v}_s = -\omega$, and as $\sigma \to 0$ it is uniformly distributed in that plane (no k,ω dependence).

As a check on these computations, Parseval's theorem is invoked:

$$\begin{aligned} P &= \iiint \left|G_s(\bar{k},\omega)\right|^2 d\bar{k}\,d\omega \\ &= \iiint \frac{\sigma^4 A_s^2 T^2 e^{-\sigma^2 \bar{k}\bullet\bar{k}}}{2\pi} \operatorname{sinc}^2\left[\left(\bar{k}\bullet\bar{v}_s + \omega\right)\frac{T}{2}\right] d\bar{k}\,d\omega \quad . \end{aligned}$$

For simplicity, set $v = 0$ so that

$$P = \iiint \frac{\sigma^4 A_s^2 T^2 e^{-\sigma^2 \bar{k}\cdot\bar{k}}}{2\pi} \operatorname{sinc}^2\left(\frac{\omega T}{2}\right) d\bar{k}\, d\omega$$

$$= \frac{1}{2}\sigma^2 A_s^2 T^2 \int \operatorname{sinc}^2\left(\frac{\omega T}{2}\right) d\omega \quad .$$

If there are many frames ($T >> p_t$) the signal is confined primarily to the single plane of width $\delta\omega = 2\pi/T$ and sinc(0) = 1 so that the integral goes to $2\pi/T$ and $P = \pi\sigma^2 A_s^2 T$, which agrees with the value derived previously in the space-time domain. A similar development for the Fourier spectrum of the stars yields:

$$G_\xi(\bar{k},\omega) = \frac{1}{\sqrt{2\pi}^3} \int_{-T/2}^{+T/2} \iint_{-\infty}^{+\infty} \sum_i A_i e^{-\frac{\left(\bar{x}-\bar{x}_i(t)\right)^2}{2\sigma^2}} e^{-i\bar{k}\cdot\bar{x}-i\omega t}\, d\bar{x}\, dt$$

$$= \frac{\sigma^2 \sum_i A_i e^{-i\bar{k}\cdot\bar{x}_i}\, e^{-\frac{\sigma^2 \bar{k}\cdot\bar{k}}{2}}}{\sqrt{2\pi}} \int_{-T/2}^{+T/2} e^{-i\left(\omega+\bar{k}\cdot\bar{v}_\xi\right)t} dt$$

$$G_\xi(\bar{k},\omega) = \frac{\sigma^2 \sum_i A_i T e^{-i\bar{k}\cdot\bar{x}_i}\, e^{-\frac{\sigma^2 \bar{k}\cdot\bar{k}}{2}}}{\sqrt{2\pi}} \sigma_{\iota\nu\psi}\left[\left(\omega+\bar{k}\cdot\bar{v}_\xi\right)\frac{T}{2}\right] \quad . \qquad (14)$$

Assuming no correlation between the stars,

$$\left|G_\xi(\bar{k},\omega)\right|^2 = \frac{\sigma^4 \sum_i A_i^2 T^2 e^{-\sigma^2 \bar{k}\cdot\bar{k}}}{2\pi} \operatorname{sinc}^2\left[\left(\omega+\bar{k}\cdot\bar{v}_\xi\right)\frac{T}{2}\right] \quad . \qquad (15)$$

If $\sigma \to 0$ such that $\sigma^2 \to A_i B_i$, then

$$\left|G_\xi(\bar{k},\omega)\right|^2 = \frac{\sum_i B_i^2 T^2}{2\pi} \operatorname{sinc}^2\left[\left(\omega+\bar{k}\cdot\bar{v}_\xi\right)\frac{T}{2}\right] \quad .$$

Like the satellite, the signal is maximized in the $\bar{k}\cdot\bar{v} \approx -\omega$ plane:

$$\left|G_\xi\left(\bar{k}\cdot\bar{v}_\xi = -\omega\right)\right|^2 \approx \left(\sum_i B_i^2\right)\frac{T^2}{2\pi} = \left(\sum_i B_i^2 T\right)\Big/\delta\omega \quad .$$

The noise Fourier power spectrum will have a constant component due to the Poisson fluctuations, as well as a zero frequency spike corresponding to the space-time average value, η. The fluctuations contribute

$$\left|G_\eta(\bar{k},\omega)\right|^2 = \frac{1}{\sqrt{2\pi}^3}\iiint R_\eta(\bar{\chi},\tau)e^{-i\bar{k}\cdot\bar{\chi}-i\omega\tau}d\bar{\chi}\ d\tau$$

$$= \frac{\rho^2 v_s}{v_f} = \frac{\rho_p^2}{v_f} \quad , \tag{16}$$

and the constant component contributes a zero frequency Fourier amplitude spike:

$$\left|G_\eta(0,0)\right|^2 = \frac{\overline{\eta}^2 V_s}{v_f} \quad .$$

Combining these two, the Fourier volume noise power spectrum is

$$\left|G_\eta(\bar{k},\omega)\right|^2 = \frac{\rho^2 v_s}{v_f} + \frac{\overline{\eta}^2 V_s}{v_f}\ \delta(\bar{k},\omega) \quad .$$

Integrating over the Fourier volume V_f gives $P = \overline{\eta}^2 V_s + \rho^2 V_s$ as in the space-time domain. Characteristic of white noise is that the power spectrum is a constant (except for the zero frequency component) independent of location in the Fourier volume. Also noted is that while the Fourier signal power components rise as T^2, the average noise contribution only rises as T.

2.4 CLUTTER SUPPRESSION

Before performing the signal enhancement operation, one must eliminate background clutter. The optimal method is a maximum likelihood-derived normalizer. Because a detailed discussion and results are given elsewhere by Pohlig [9], this report will only present some brief results using the normalizer as a front end clutter suppression algorithm. The normalizer determines the average and standard deviation of the pixels at each spatial location (a pixel-by-pixel average over time) and then for each frame replaces the value by [value – average/standard deviation]^2.

$$I_{i,j,k} = \left[\frac{I_{i,j,k} - \bar{I}_{i,j}}{\sigma_{i,j}}\right]^2 \quad . \tag{17}$$

This procedure removes any fixed patterns in the image (stars, fixed pattern noise, etc.). Because the stars represent statistically nonstationary noise (due to their larger Poisson contribution), the normalizer has the

desirable effect of restoring stationary statistics. However, if one uses all N_t time samples to define the mean and standard deviation, the resulting data exhibit a β distribution [10], while if one excludes the current temporal value and uses the remaining N_t-1 samples, the data exhibit an F distribution. If one uses the F distribution approach, the "normalized" data are in fact simply a map of the single pixel SNR.

Alternatively, stars can be thought of as a structured noise component to be removed by the matched filter. In this case, the $|N(\omega)|^2$ term in the matched filter description contains both the white background noise and the star contribution:

$$\left|N(\bar{k},\omega)\right|^2 = \left|G_\xi(\bar{k},\omega)\right|^2 + \left|G_\eta(\bar{k},\omega)\right|^2 \quad .$$

Using this description in the matched filter essentially notches out the intersection of the spectral plane of the stars with that of the satellites. The equations of the two planes are

$$\bar{k}\bullet\bar{v}_\xi = -\omega$$

$$\bar{k}\bullet\bar{v}_s = -\omega \quad ,$$

and the line of intersection of the two planes computed is

$$\bar{k}\bullet\bar{v}_\xi = \bar{k}\bullet\bar{v}_s \quad ,$$

$$k_y = \frac{v_{\xi_x} - v_{s_x}}{v_{s_y} - v_{\xi_y}}\, k_x \quad .$$

These computations can efficiently separate a moving object from stars that are moving at a different velocity. (This technique works equally well in ephemeris track or sidereal mode.) In practice, one would simply remove the star plane and then test with the candidate velocity filters rather than weighting each velocity filter for the intersection line. Unfortunately, a bright star located on a pixel boundary and subject to small position fluctuations generates large random intensity variations that are spread throughout the Fourier volume and consequently cannot be removed. Even if no jitter were present, the stars would still exhibit random intensity fluctuations due to the Poisson nature of the photon arrival statistics.

The use of a star catalog combined with the telescope line of sight to produce a star mask can remove stars to the 14th magnitude. This approach is extremely powerful and overcomes the limitations of the preceding method by introducing additional information. Because one sets the area of the star to the average background, minor star motion and resulting fluctuations, as well as Poisson noise, can be completely eliminated without significantly disturbing the noise statistics. Unlike the previous method however, the star map does not remove any fixed pattern noise. If this noise presented a problem, the star map could easily be combined with a zero frequency notch filter to add fixed pattern suppression.

2.5 ANALYSIS AND DETECTION

The dark current white noise is uniformly distributed throughout the Fourier volume (except for the zero frequency spike). The signal due to stars is maximized in the $\bar{k} \bullet \bar{v}_\xi = -\omega$ plane, while the signal from a satellite is maximized in the $\bar{k} \bullet \bar{v}_s = -\omega$ plane. In both cases the signal is maximized in the indicated plane and falls off as a sinc function on both sides. The longer the data collection time, the better the signal is confined to the plane. For an infinite streak the signal is contained entirely within a single plane, while for a short streak the sinc function can have significant power in some of the lobes. An infinitesimal cross section for a streak (single pixel width) leads to uniform intensity in the main signal plane. As the signal smears out, either due to saturation of the detector, atmospheric jitter, or resolution of an object, the intensity distribution in the plane loses its uniform characteristic.

While it is fairly obvious that the signal is maximized in the $\bar{k} \bullet \bar{v}_s = -\omega$ plane, there are sidelobes; it would be useful to know their amplitude and extent. In general, the signal in the Fourier volume is

$$\left|G_s(\bar{k},\omega)\right|^2 = \frac{\sigma^4 A_s^2 T^2 e^{-\sigma^2 \bar{k} \bullet \bar{k}}}{2\pi} \; sinc^2\left[\bar{k} \bullet \bar{v} + \omega)\frac{T}{2}\right] \quad .$$

As long as $\sigma|\bar{k}| << 1$, the functional dependence is entirely within the sinc function. For a discretely sampled image volume let $\bar{k} \rightarrow \bar{m} 2\pi/L$, $\omega \rightarrow \eta 2\pi/T$, thus rewriting the sinc function (and defining $\delta k = 2\pi/L$, $\delta\omega = 2\pi/T$):

$$\frac{\sin\left(\frac{\bar{m}\delta k v T}{2} + \frac{n\delta\omega T}{2}\right)}{\frac{m\delta k v T}{2} + \frac{n\delta\omega T}{2}} = \frac{\sin\left(\frac{\bar{m}\pi v T}{L} + n\pi\right)}{\frac{m\pi v T}{L} + n\pi} = \frac{\sin\left(\frac{\bar{m}\pi v T}{L}\right)}{\frac{m\pi v T}{L} + n\pi} \quad , \tag{18}$$

which is not very interesting; however, if $\nu = 0$,

$$\left|G_s(\bar{v}=0)\right|^2 = \frac{\sigma^4 A_s^2 T^2 e^{-\sigma^2 \bar{k} \cdot \bar{k}}}{2\pi} \; \mathrm{sinc}^2\left(\omega\frac{T}{2}\right) \quad .$$

In this case the sinc function becomes

$$\mathrm{sinc}\left(\omega\frac{T}{2}\right) = \mathrm{sinc}\left(n\delta\omega\frac{T}{2}\right) = \mathrm{sinc}(n\pi) = 0 \qquad n = 1,2,3,\ldots \quad .$$

Thus all pixels are zero except at $\omega = 0$, those exactly in the plane. For objects with $|\bar{v}| = 0$, such as stars in sidereal tracking mode, the signal is confined entirely to the $\omega = 0$ plane.

Expression (18) shows that for $\bar{v} > 0$, the signal falls off in the ω dimension with a $1/n$ dependence, and in fact a significant amount of the signal power can lie outside the primary signal plane, implying that approximations, assuming the signal is confined to a single plane, can be seriously in error.

In the spatial domain the energy per pixel [Equation (4)] for $|\bar{v}_s|\rho_t > \rho_x$ was

$$e_s = \frac{2\pi B_s p_x}{|\bar{v}_s|} \quad ,$$

and so the single pixel SNR is

$$\mathrm{SNR}_s = \frac{2\pi B_s p_x}{|\bar{v}_s|\rho_p} \quad . \tag{19}$$

The matched filter operation integrates the entire energy of the object for a total signal strength of $E_s = 2\pi B_s T$. The total noise energy (above the mean) contained in this streak is

$$\langle E_\eta \rangle = \sqrt{\eta v_s \Omega} = \rho_p \sqrt{\frac{|v_s| p_t N_t}{p_x}}$$

so that the output single pixel SNR from the matched filter (after back transforming) is

$$\mathrm{SNR}_f = \mathrm{SNR}_s \sqrt{\Omega} = \frac{2\pi B_s}{\rho_p} \sqrt{\frac{p_x T}{|v_s|}} \quad . \tag{20}$$

With this operation, one can set a detection threshold a desired number of standard deviations (α) above the noise mean. The detection criterion on the filtered signal (E_s) is then $E_s > \alpha \langle E_\eta \rangle$. Using Gaussian statistics the P_d and P_{fa} can now be derived. For a Gaussian distribution with standard deviation $\lambda = \rho_p \Omega$, the probability of observing a noise contribution greater than $\alpha\lambda$ is

$$P_{fa}(\alpha) = \frac{1}{\sqrt{2\pi}\lambda} \int_{\alpha\lambda}^{+\infty} e^{-\frac{x^2}{2\lambda^2}} dx = \frac{1}{\sqrt{\pi}} \int_{\alpha/\sqrt{2}}^{+\infty} e^{-z^2} dz = \frac{1}{2}\mathrm{erfc}\left[\frac{\alpha}{\sqrt{2}}\right] \quad , \tag{21}$$

where erfc(x) is the complementary error function normalized such that erfc(0) = 1. The system P_{fa} (for one data set) is $1 - (1 - P_{fa})N_x N_y N_t \approx P_{fa} N_x N_y N_t$. The probability of detecting a signal of strength E_s embedded in this noise is:

$$P_d(E_s) = 1 - \frac{1}{\sqrt{2\pi}\lambda} \int_{E_s - \alpha_\lambda}^{+\infty} e^{-\frac{x^2}{2\lambda^2 dx}} \qquad E_s > \alpha\lambda$$

$$P_d(E_s) = \frac{1}{\sqrt{2\pi}\lambda} \int_{\alpha\lambda - E_s}^{+\infty} e^{-\frac{x^2}{2\lambda^2 dx}} \qquad E_s < \alpha\lambda \quad ,$$

which may be written

$$P_d(\mathrm{SNR}_f,\alpha)=\frac{1}{2}+\frac{1}{2}\ \mathrm{erf}\left[\frac{E_s-\alpha\lambda}{\sqrt{2\lambda}}\right]=\frac{1}{2}+\frac{1}{2}\ \mathrm{erf}\left[\frac{\mathrm{SNR}_f-\alpha}{\sqrt{2}}\right] \qquad \mathrm{SNR}_f>\alpha \quad (22a)$$

$$P_d(\mathrm{SNR}_f,\alpha)=\frac{1}{2}\mathrm{erfc}\left[\frac{\alpha\lambda-E_s}{\sqrt{2\lambda}}\right]=\frac{1}{2}\ \mathrm{erfc}\left[\frac{\alpha-\mathrm{SNR}_f}{\sqrt{2}}\right] \qquad \mathrm{SNR}_f<\alpha \quad . \quad (22b)$$

Using Equations (21) and (22), families of receiver operator curves (ROCs) can be generated, representing P_d as a function of the filtered SNR for fixed P_{fa}. Because the filtered SNR is just $\mathrm{SNR}_f = \mathrm{SNR}_s\sqrt{\Omega}$, one can easily determine P_d at a given P_{fa} for a desired SNR_s and velocity, which is shown as a single curve in Figure 3. To use this, one determines the input single pixel SNR and the candidate velocity, from which one computes the filtered SNR ($\mathrm{SNR}_f = \mathrm{SNR}_s\sqrt{\text{streak length}}$). Then for a desired threshold α (false alarm rate), the abscissa is determined and the P_d may then be read off the graph.

In digital electronic implementations, Fourier transforms are relatively expensive operations; one might ask if detection is possible in the Fourier volume, thereby eliminating the need for the inverse transform. While the noise adds incoherently, the signal must add coherently with a phase factor that varies from point to point. The calculation of this phase factor and the subsequent coherent addition is nothing less than the inverse transform; thought of another way, the noise density remains constant through the transform; however, the signal is transformed from a one-dimensional line to a two-dimensional plane. Thus the single pixel SNR is actually lower in the Fourier volume.

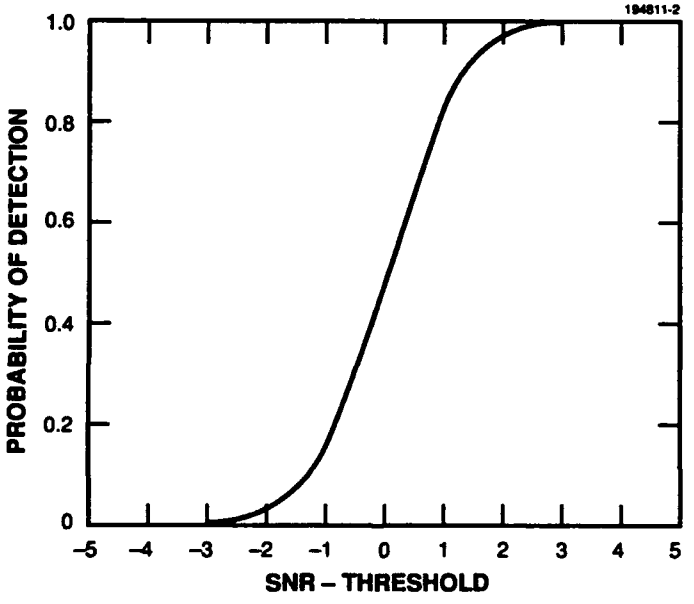

Figure 3. General detection curve, fixed P_{fa}.

3. RESULTS

3.1 SIMULATION SNR ENHANCEMENT AND P_d, P_{fa}

A three-dimensional matched filtering package was written in C to run under Unix and X-Windows/Motif. The heart of the package is an *n*-dimensional fast Fourier transform algorithm adapted from *Numerical Recipes* [11]. One should be aware that the results of a fast fourier transform (FFT) are folded in frequency space as described below. Wells et al. [12] give a good description of the data geometry involved in three-dimensional transforms. While the ultimate goal is to process real data sets, it is important to be able to generate synthetic data having known properties to verify the model, the algorithm, and its understanding under controlled circumstances. Therefore a test pattern-generating program was developed that generates three-dimensional data sets composed of Gaussian white noise having a specified mean and standard deviation. To this may be added constant intensity objects moving at specified velocities and randomly placed single pixel events corresponding to gamma ray bombardment effects. The objects would correspond to satellites or stars and have velocities in any direction or zero (corresponding to stars in the sidereal case) with different brightness levels to simulate the intensity difference between typical stars and satellites. The program can generate image sets using either a δ-function PSF or Gaussian PSF. Typical image sets using existing CCD cameras and electronics are digitized to 12 bits, yielding a 0- to 4,095-pixel gray scale. A typical noise mean is 734 with a standard deviation of 7.3. Stars can take on values anywhere up to 4,095 and can, in fact, saturate the detector causing several nonlinear and multipixel effects that are beyond the scope of this report. Similarly, satellites can have single pixel SNR values from <1 to >10. The single pixel SNR is measured according to (value – average)/standard deviation. The SNR of a star is referred to as the clutter-to-noise ratio, or CNR.

Several performance demonstrations are shown using two-dimensional images because they are easier to display on paper and simple to comprehend. Figure 4 shows a two-dimensional streak of constant intensity superimposed on a white noise background. A matched filter was generated by forming a two-dimensional streak of the same length located at the origin (lower left) in a field with no noise. Figure 5 shows the result of performing an FFT on the image and the filter, multiplying the two, and then performing an inverse FFT. The result is the expected convolution of two rectangle functions: a triangle function. The center of the triangle will actually appear at the location of one end of the streak in Figure 4, but the matched filter arbitrary phase factor was used to move the output peak to the center of the original streak. If this process is performed with streaks of various lengths, then the data shown in Figure 6, which follows the theoretical curve quite well, is obtained, thus verifying this model and its implementation.

As the study moves to full three-dimensional data sets, one of a number of problems that arises is how to view and represent the data. Typically, each data frame (representing a constant time slice) is viewed as an *x,y* grid. In this case time forms the third axis. One must decide whether to represent these data as a series of two-dimensional slices, as a projection, or as a color code. A maximum value projection technique is well suited to space surveillance data sets because it allows a compact (single frame) representation without a color requirement. For each (x,y) point in the three-dimensional image volume,

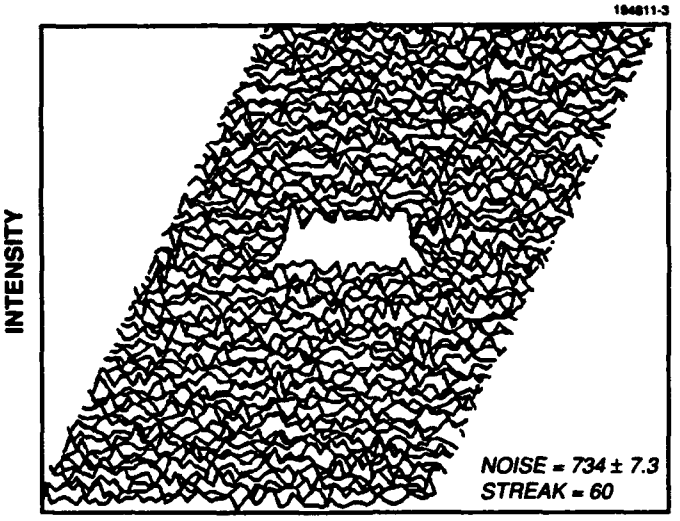

Figure 4. Original two-dimensional data: 21 pixel streak, single pixel SNR = 8.2.

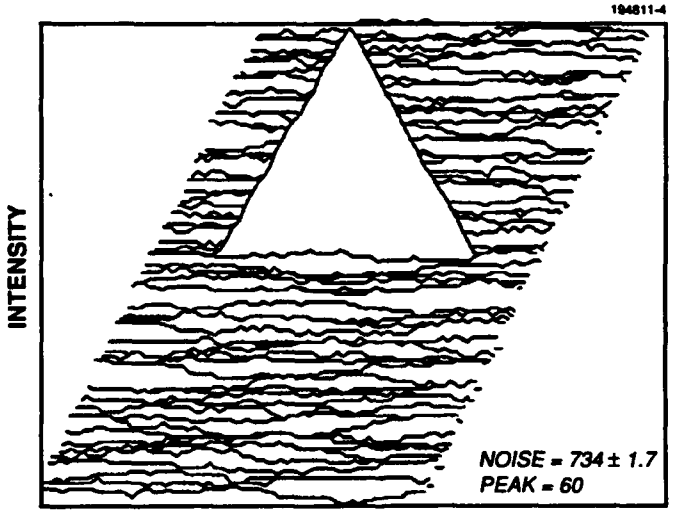

Figure 5. Two-dimensional matched filter output. Output SNR = 36.

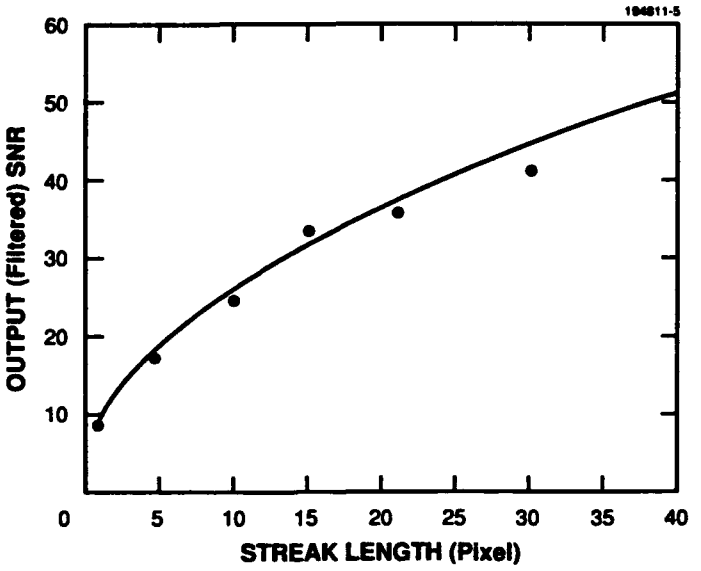

Figure 6. Two-dimensional matched filter SNR enhancement. Input single pixel SNR = 8.2.

the maximum value projection examines each data frame and uses only the maximum value to produce the output two-dimensional image frame; however, a strict maximum value projection technique suffers from modulation of a constant intensity moving object because energy is split between frames. For example, an object moving in the x direction at 1.3 pixels per frame has a brightness B_o in the first pixel but only 1/3 B_o in the second. On the next frame the second pixel has 2/3 B_o. Thus due to the energy split the second pixel shows an artificial reduction, which can be overcome by using a pairwise maximum value projection; however, this technique is generally only applicable to objects moving faster than 1 pixel per frame. The effect of the two techniques is shown in Figures 7 and 8.

An object translating parallel to the x-axis is now used to explore the Fourier volume. Upon generating an image volume and taking its Fourier transform, one finds (as predicted) that the Fourier image volume is independent of the k_y coordinate. Taking a slice through the k_x, ω plane yields the images shown in Figures 9 and 10. Two features are worth noting; instead of a single plane there are clearly two planes containing signal in this image, and the two planes are not of uniform intensity but rather exhibit a roll-off phenomenon along their length.

Figure 9 shows the in-plane roll-off due to a Gaussian PSF having $\sigma = 0.74$ pixels, which corresponds to one of Lincoln's commonly used telescopes. A δ-function PSF transforms to yield a sinc function roll-off dependent on integration time, as shown in Figure 10. The roll-off in this case may be written as $\text{sinc}[\boldsymbol{k} \bullet \overline{v}_s \rho_1 / 2]$, which may be rewritten in one dimension as $\text{sinc}[i\pi v_f / N_x]$. The first zero clearly occurs at pixel $i = N_x / v_f$.

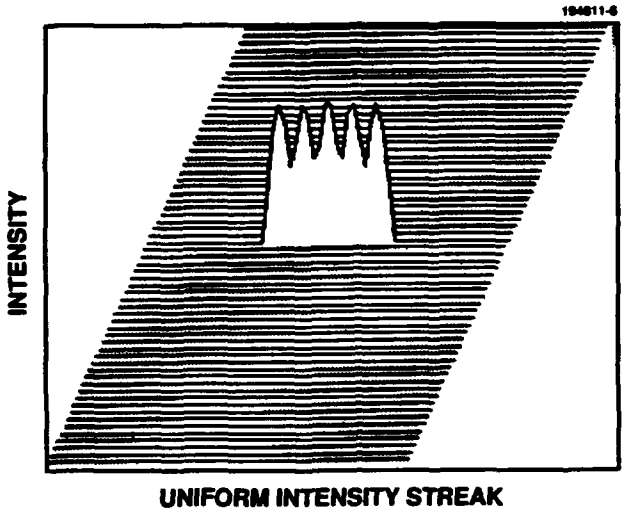

Figure 7. Sixteen-frame maximum value projection. Modulation due to energy split between frames.

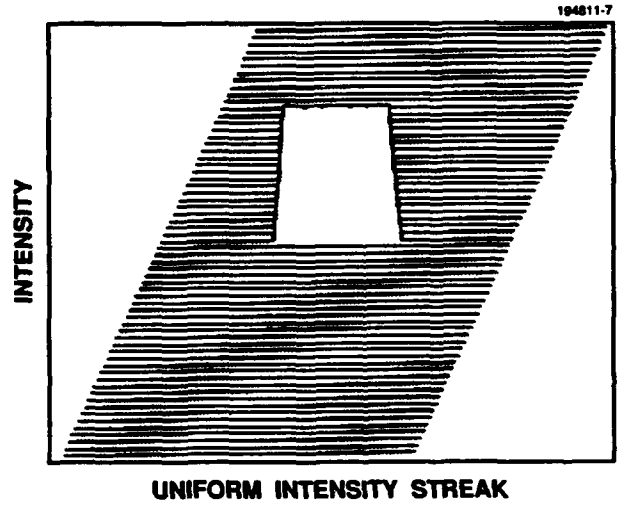

Figure 8. Sixteen-frame pairwise maximum value projection.

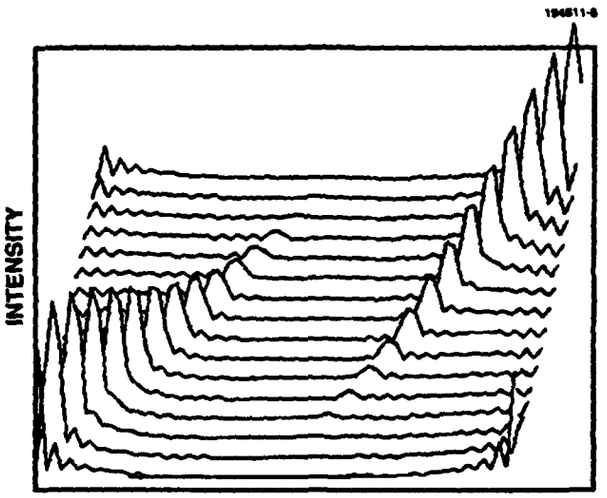

Figure 9. K_x versus w slice from Fourier volume, Gaussian PSF (σ = 0.74 pixels).

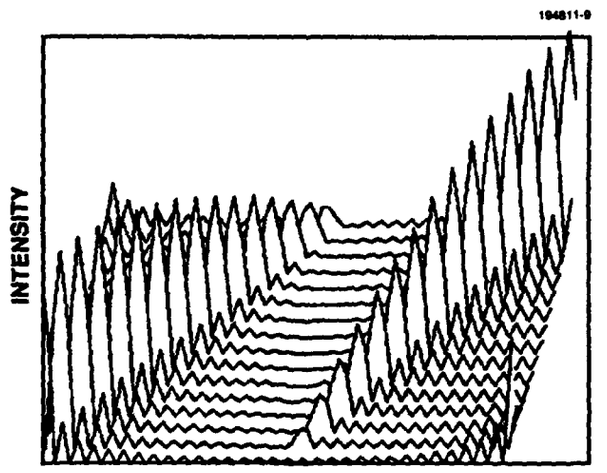

Figure 10. K_x versus w slice from Fourier volume, δ-function PSF.

The signal decreases as $\mathrm{sinc}[(\omega + \bar{k} \bullet \bar{v}_s)T/2]$ as one moves away from the primary signal plane. Thus in a constant plane the signal decreases as $\mathrm{sinc}(\delta k v_s T)/2$, putting the first zero at $(\delta k v_s T)/2 = \pi$. Using $dk_x = 2\pi/N_x p_x$, one can solve for the pixel i, which contains the first zero:

$$i = \frac{p_x N_x}{T v_s} = \frac{N_x}{N_t v_f} \quad ,$$

where $T = N_t p_t$ and $v_s = p_x v_f / p_t$ with v_f in pixels per frame. The width of the streak will be $2i$ pixels.

The signal plane that starts in the upper right corner represents the negative frequency components due to the standard Fourier space wraparound when the signal bandwidth exceeds the sampling bandwidth. In the case of a single streak, the two signals remain separated at all velocities except $v_x = 1$ pixel per frame; however, if multiple targets moving at different velocities are present, their signals will overlap. The only way to prevent this mixing of frequency components is to assure that the signal goes to zero before reaching the Nyquist frequency [13].

Generating and storing a large bank of candidate velocity filters covering the full three-dimensional image volume can be prohibitive for current mass storage technology (especially if they are needed on-line in a real-time processor). For example, a single 420 × 420 pixel × 16 frame image when transformed to a complex double precision (8 bytes) Fourier volume image requires 45 Mbytes. Storage requirements can be reduced considerably; nevertheless the data volume remains significant because a typical filter bank contains up to 1,000 filters [14]. Fortunately, an analytical expression for the Fourier volume representation of the filters is available, thus enabling computation on the fly. The particularly simple form wherein the signal is confined to a single (albeit wrapped) plane allows the Fourier volume to be set equal to zero except for the signal plane itself, which is weighted by the sinc function or Gaussian roll-off described above. The width of this plane in pixels (derived above) is $2N_x/N_t v_f$.

Synthetic three-dimensional data sets were generated, containing noise and a target moving at various velocities and with various constant intensity values. The complete matched filter operation was applied, consisting of transforming both the input data set and a filter data set, multiplying the three-dimensional Fourier volumes, and back transforming the product. As predicted, both the single pixel and the matched filter SNR increased linearly with target brightness, while the matched filter SNR increased as the square root of the target streak length (for constant brightness per pixel). Results using the full volume multiply and the analytically computed filter are presented in Figure 11 for a constant brightness per pixel target and in Figure 12 for a constant brightness target. The P_{fa} estimates for various thresholds were verified on both original and filtered data. For example, using 64 × 64 pixel × 16 frames of data, the number of false alarms as a function of the threshold α was verified to be $n = P_{fa}(\alpha) N_x N_y N_t$, and λ could be accurately estimated from the data.

The result of the the full three-dimensional matched filter is a three-dimensional data set in which the signal forms a triangle much as in the two-dimensional case (Figure 5), but now it is aligned along the target trajectory in three dimensions. A maximum value projection of this signal would in fact produce an image similar to that in Figure 5. In comparison, if the predetermined temporal plane containing the peak SNR were selected, then the two-dimensional image shown in Figure 13 would be

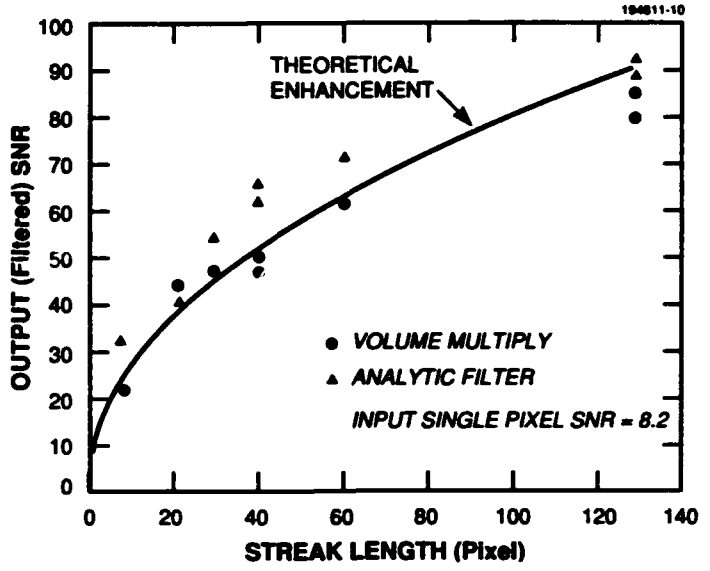

Figure 11. Comparison of analytic matched filter with volume multiply for constant input SNR.

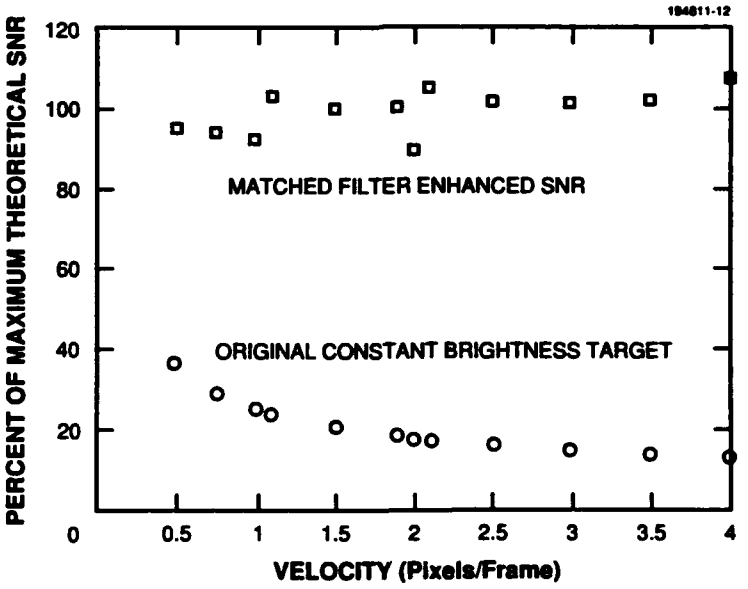

Figure 12. SNR enhancement as a percent of theoretical δ-function PSF.

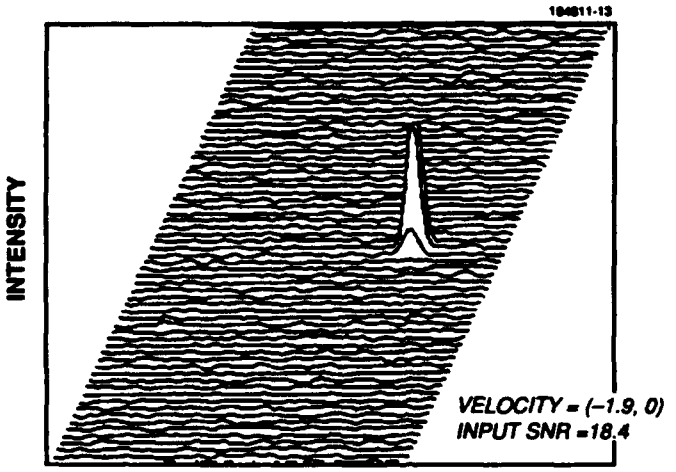

Figure 13. Two-dimensional SNR peak frame result.

obtained. This result is a single frame of data as opposed to the full matched filter three-dimensional data set, and the signal peak is much narrower; it is a triangle twice the width of the single frame motion ($2v'$) rather than a triangle twice the width of the entire data set motion ($2v'N_f$). The matched filter arbitrary phase factor has been used to position the signal peak in frame $N_f/2$, frame 8, for the current 16-frame data sets. This procedure was used to minimize wraparound effects.

Using synthetic images with no jitter or Poisson noise effects, the Fourier star slice removal technique produced excellent results. The stars were completely eliminated with no residual artifacts. The impact on further processing, specifically the signal enhancement filtering, was negligible. It was found that for all but the lowest velocity objects the output SNR was not affected. At very low velocities the star and signal planes begin to have a significant intersection volume leading to signal reduction in the final output.

3.2 REAL DATA SNR ENHANCEMENT AND P_d, P_{fa}

The model assumes point objects moving with no intensity variation (signature or Poisson) and no positional errors (jitter). In reality both effects are present, meaning that one should expect some discrepancies between the model and reality. For example, the Fourier domain star notch filter will not completely remove the stars, and the output signal from a detected satellite will no longer have the nice triangular form seen in the simulated data. In this section an initial attempt is made to translate the preceding theoretical results to real data.

An interesting and representative data set, labeled "geo.dat," having an average background level of 709.7 with a Gaussian distribution noise of $\sigma = 9.1$, was used. Several stars are present with intensities ranging up to our 12-bit limit of 4,095. There are two geosynchronous satellites present in the image set,

one relatively bright object and one extremely faint. For ease of processing this data set was clipped to form two data sets of 64 × 64 pixels × 16 frames each. They were labeled "geob.dat" to denote the data set containing the bright streak and "geow.dat" to denote the data set containing the faint streak. During the data collection process a constant bias current is added to the analog current prior to the analog-to-digital converter. To relate the peak values of objects such as stars to their Poisson noise, the bias must first be subtracted. For the image set geo.dat this bias had a digital value of 601.

A maximum value projection of the bright streak image set is shown in Figure 14, while Figure 15 is a histogram of the noise distribution. There are five stars visible in this image. Using a brightness (row, column) notation: 4,095 (56,50); 1,228 (48,51); 2,710 (28,56); 1,164 (22,23); and 1,124 (37,36). The streak has a maximum single pixel value of 1,026 and an average value 901. Using the value of 901 gives an SNR = 21.1. The streak profile also reveals variations (standard deviation = 53) grossly in excess of background noise level fluctuations due to frame-to-frame energy splitting. Figure 16 shows the Fourier volume (closely resembling Figure 9), the image of which corresponds to a Gaussian PSF ($\sigma = 0.74$ pixels). In this instance the star map has been applied to eliminate the stars, followed by a Fourier transform.

An examination of the stars reveals that the standard deviation computed for a time sequence of pixels containing a star is typically two to three times greater than predicted using $\sqrt{\text{average} - \text{bias}}$. The origin of these fluctuations appears to be atmospheric or mount-related jitter causing the high gradient star PSFs to move across pixel boundaries.

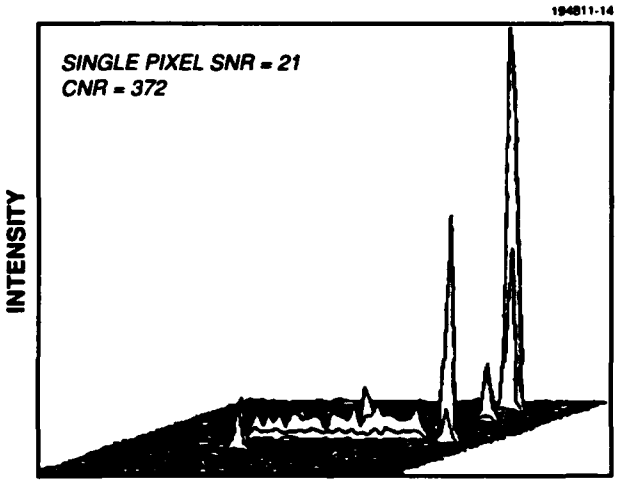

Figure 14. Original image data set, maximum value projection.

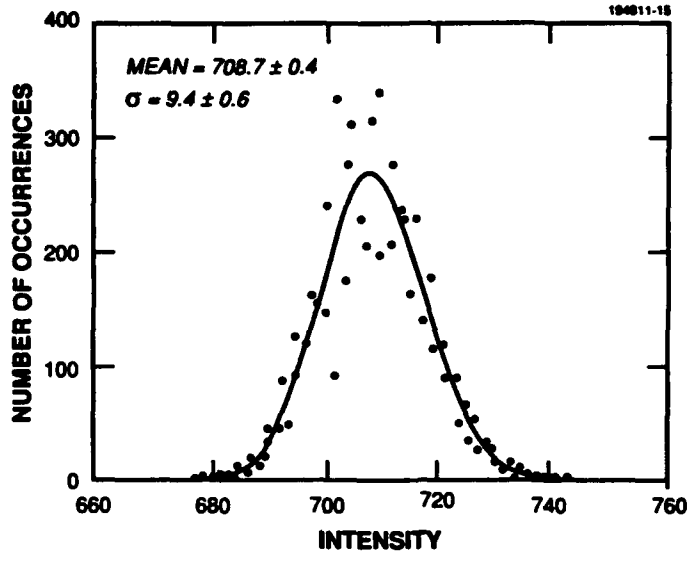

Figure 15. Nonlinear least squares Gaussian fit of original data.

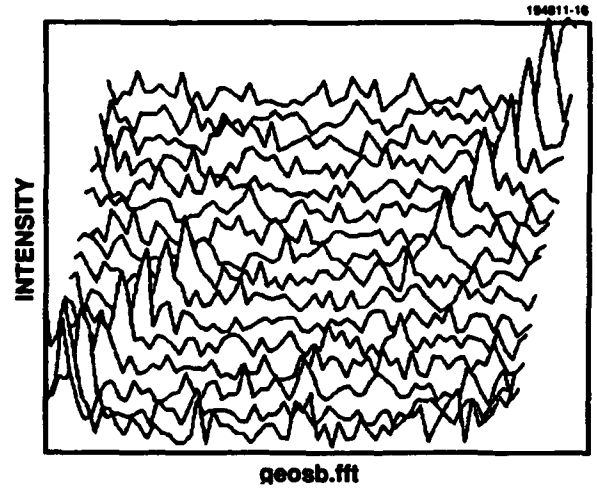

Figure 16. Fourier transform of geosb.dat bright streak. Star map clutter suppression applied.

The results of the clutter suppression algorithms are shown in Figures 17 through 19. The star slice removal algorithm reduces but does not eliminate the stars, while the normalizer produces a map of single pixel SNR. CNR is computed using (4,095 – 709.7)/ 9.1 = 372.

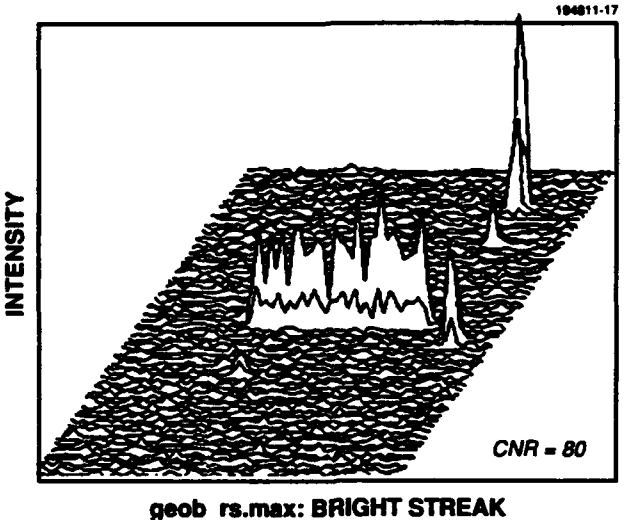

Figure 17. Clutter suppression: Fourier star slicer applied, maximum value projection.

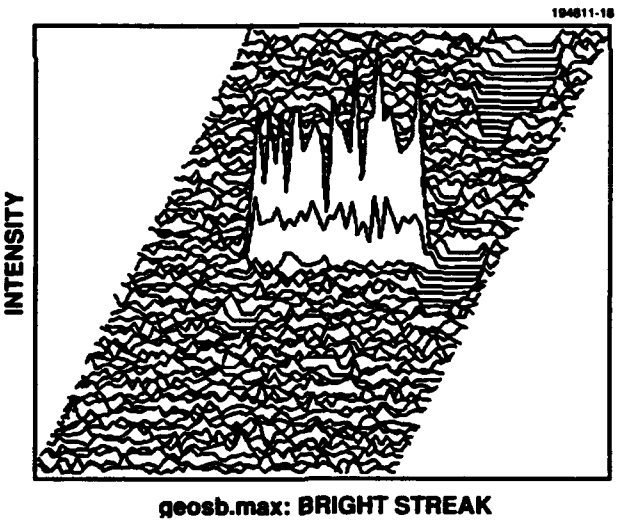

Figure 18. Clutter suppression: star map mask applied, maximum value projection.

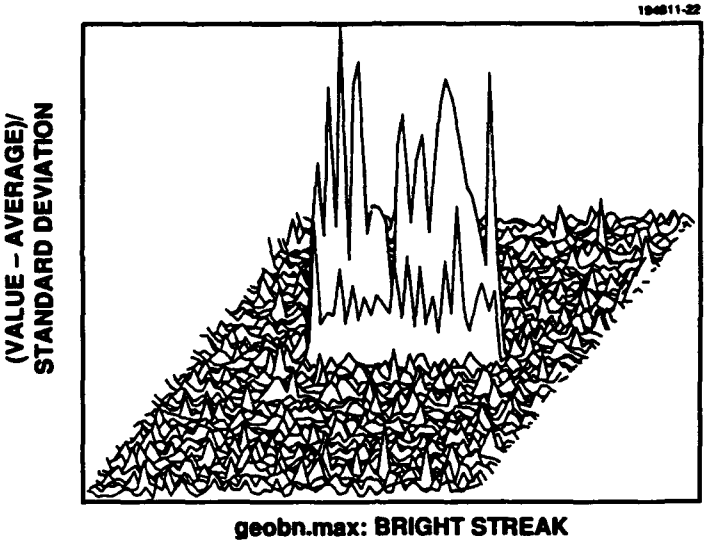

Figure 19. Clutter suppression: maximum likelihood normalizer (F statistics) maximum value projection.

Examining the original data shows a streak length of 31 pixels, which corresponds to $v_x = -1.94$ pixels/frame and $v_y = 0$. After applying the matched filter for signal enhancement, the final images shown in Figures 20 through 22 and summarized in Table 1 are obtained. These figures represent the pairwise maximum value projection of the full three-dimensional result. In this case the enhanced SNR is sufficiently large that peak shifting due to noise presents no problem. The two-dimensional result obtained using only the peak output frame (corresponding to the shift-and-add result) is shown in Figure 23 for normalizer clutter suppression, corresponding to Figure 22. The values for signal and star peak represent the image values with the background average subtracted. The enhanced SNR is expected to be the single pixel SNR multiplied by the square root of the streak length: $SNR_{en} = SNR_{sp}\sqrt{vN_t} = 5.5\ SNR_{sp} = 116$. Both the results in Table 1 and Figures 20 through 22 confirm that all three methods yield good agreement with theory; however, the star slice clutter suppression method does allow some leakage (upper right corner of Figure 20). A binary threshold may be applied to obtain a clean detection using any of these results.

The faint streak image set has an average noise level of 713.6 with a standard deviation of 9.7. Two stars are visible in the image: 2108 (20,57) and 896 (25,60). Several significantly weaker stars are also present. The streak, while present horizontally in the center of the image, is completely indiscernible. A maximum value projection of the original image set is presented in Figure 24. Figures 25 through 27 show the result of the various clutter suppression techniques followed by the matched filter. In this case a series of filters was used. The best output SNR was obtained using $v_x = -1.55$ pixels/frame and $v_y = 0$, corresponding to a streak length of 25 pixels (see Table 2).

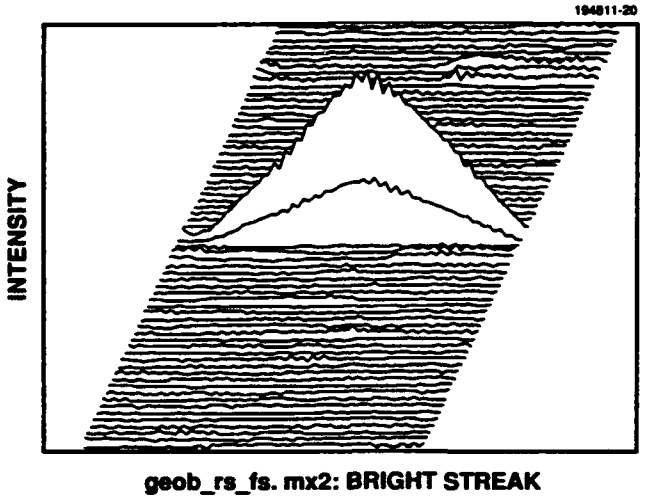

Figure 20. Fourier star slice + matched filter.

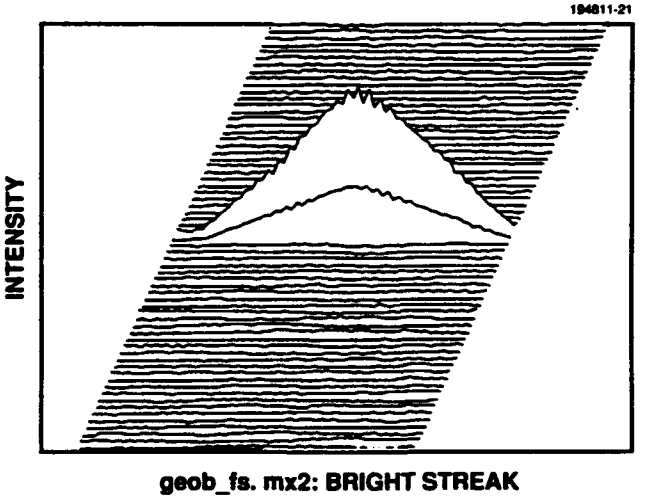

Figure 21. Star map + Fourier matched filter.

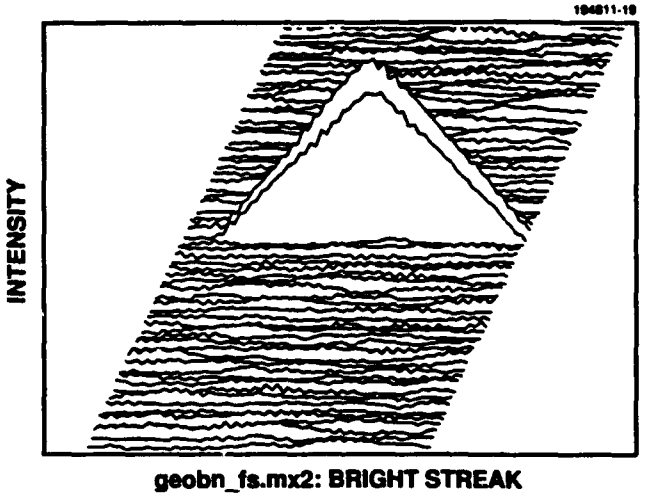

Figure 22. Maximum likelihood normalizer + Fourier matched filter.

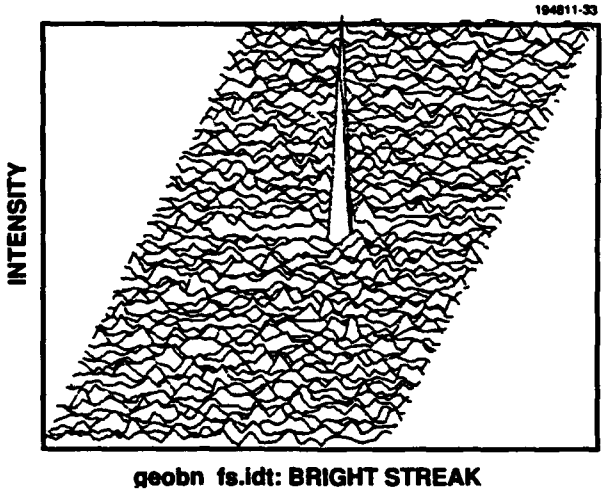

Figure 23. Peak output frame: maximum likelihood normalizer + Fourier matched filter.

TABLE 1

geob.dat Bright Streak*

	Signal	Noise	% Theoretical SNR		Star Peak	Star CNR
Original data	192	9.1	21.1		3386	372
Star map + filter	164	1.33	123.2	106.6	0	0
Star slice + filter	164	1.36	120.4	103.5	15.4	11.3
Normalizer + filter	219	2.00	109.7	94.3	0	0

*Length = 31 pixels

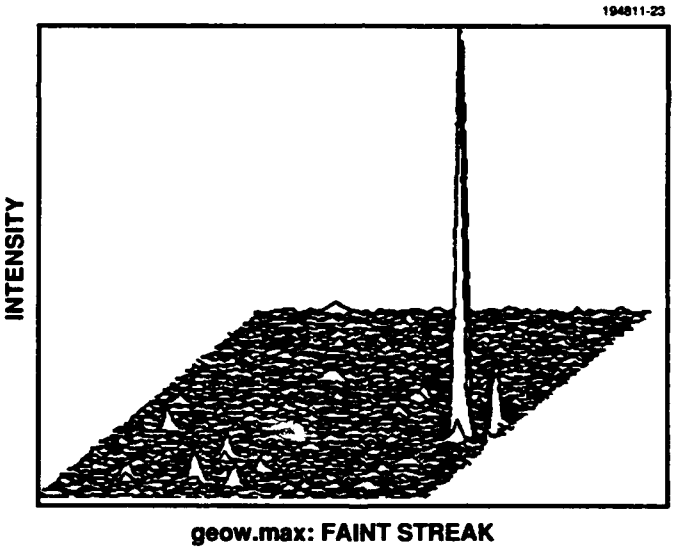

Figure 24. Original image data set, maximum value projection.

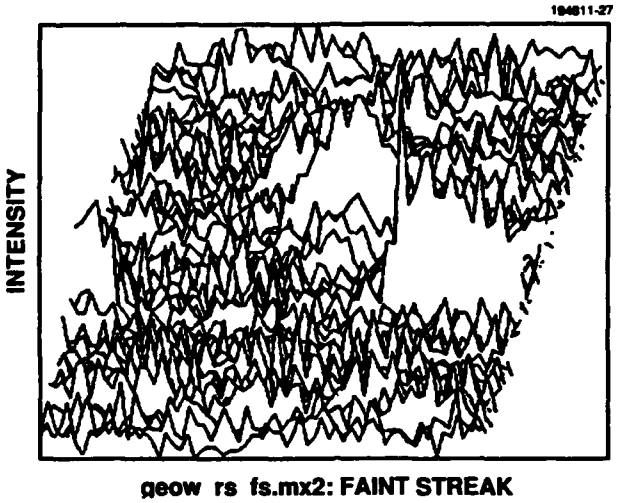

Figure 25. Fourier star slice + matched filter, pairwise maximum value projection.

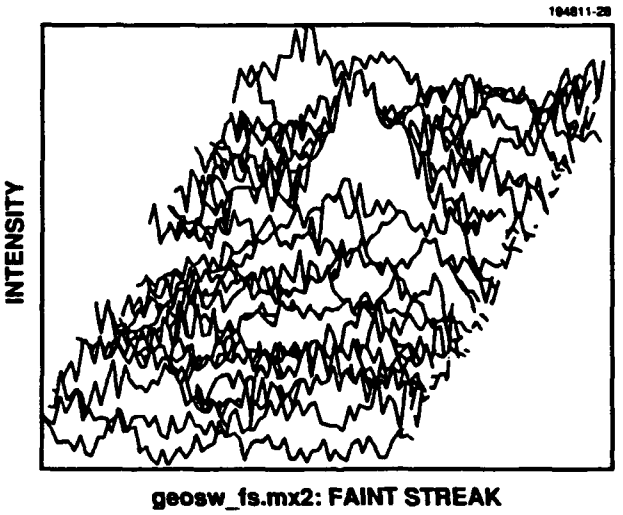

Figure 26. Star map + Fourier matched filter, pairwise maximum value projection.

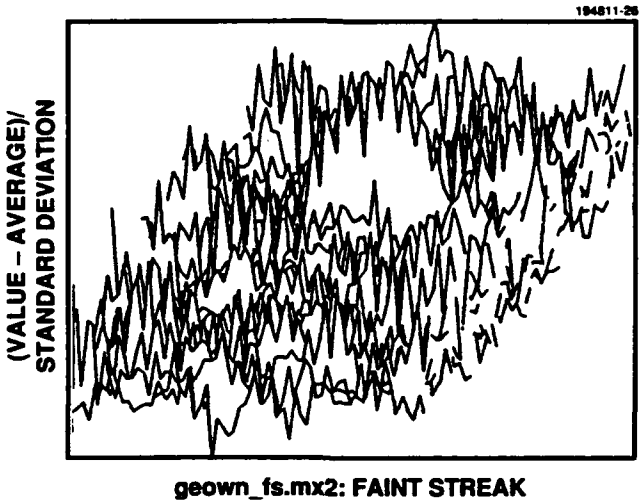

Figure 27. Maximum likelihood normalizer + Fourier matched filter, pairwise maximum value projection.

TABLE 2

geow.dat Faint Streak*

	Signal	Noise	SNR	Star Peak	Star CNR
Original data		9.66		1394	139
Star map + filter	10.5	1.22	8.5	0	0
Star slice + filter	10.1	1.14	8.8	12.8	11.2
Normalizer + filter	1.39	0.24	5.8	0	0

*Length = 25 pixels

As with the bright streak, the normalizer and the star map completely remove all the stars, including many of low intensity, while the Fourier star notch filter dramatically reduces the star intensities but fails to completely suppress them. In this case the residual star contribution is brighter than the enhanced streak. The original target is too faint to measure the SNR directly; however, working backwards from the detection the unprocessed SNR is estimated to be between 1 and 1.7.

To achieve detection a binary threshold ($\alpha = 4$) is applied to the filter output to obtain Figures 28 through 30. Comparing the three detection images it is seen that using the a priori threshold, only the star map method gives a clean detection. The star slice gives a strong detection but also detects residual star energy. The normalizer also shows a strong detection but is accompanied by many random false alarms. By experimentally adjusting the threshold ($\alpha = 3$), the star map and the normalizer give a clean detection (Figure 31). The star slice technique has dramatically reduced the star contribution, but it remains the brightest feature in the image set, and thus a clean detection is not possible. Based on Figures 26 and 27, while the star map and the normalizer give clean detections, it appears that the star map gives a "stronger" detection.

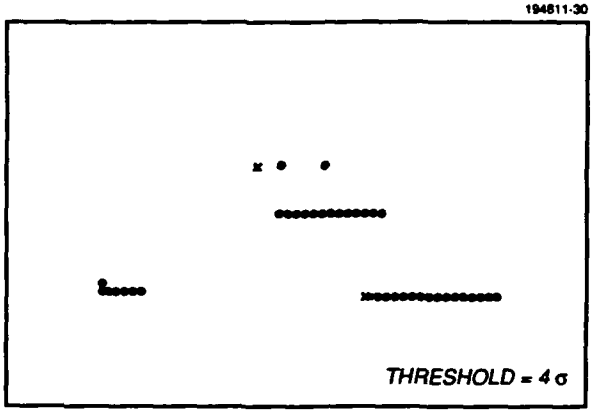

Figure 28. Threshold image: Fourier star slice + matched filter.

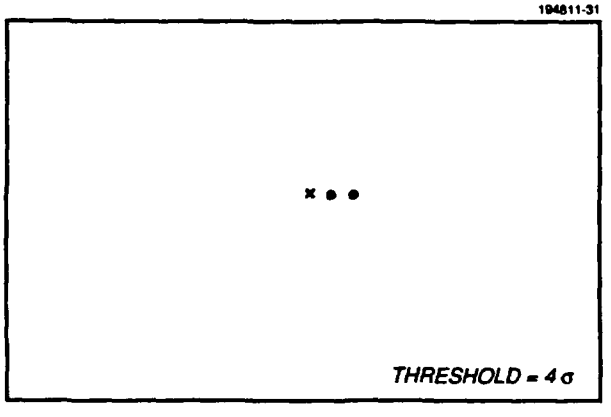

Figure 29. Threshold image: star map + matched filter.

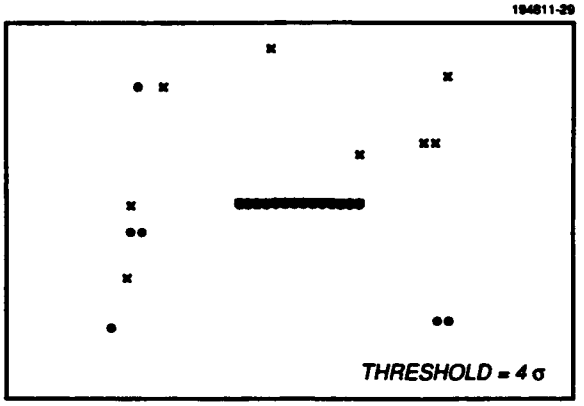

Figure 30. Threshold image: normalizer + matched filter.

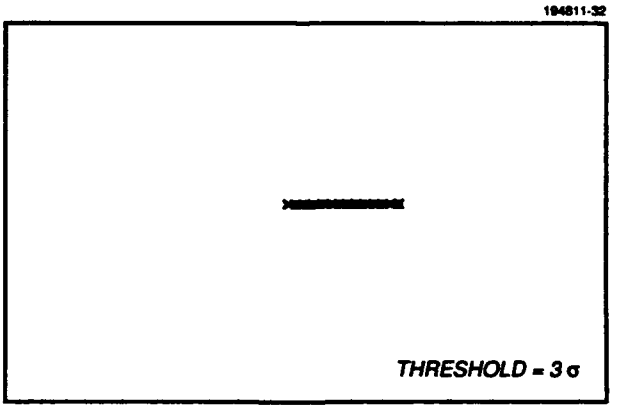

Figure 31. Threshold image: star map.

4. SUMMARY

A model of image sets used in space surveillance applications has been generated from which a three-dimensional Fourier matched filter theory has been developed and tested. SNR enhancement, P_d, and P_{fa} have been computed. Three clutter suppression algorithms for star removal have also been examined and compared. Results using synthetic computer-generated data and real data agree extremely well with theoretical predictions, as do preliminary results using actual field data.

Although the star slice method for clutter suppression does not completely eliminate the stars, it can reduce them to a level less than all but the faintest objects; it can also eliminate all objects moving at a fixed velocity, which is an advantage. Two other star removal techniques completely eliminate the stars but have added drawbacks. A star map mask, using a star catalog and the telescope line of sight, is computationally expensive but preserves the underlying statistics. This approach achieves high performance by bringing additional a priori information to the process. A maximum likelihood normalizer can be efficiently implemented, and for stationary (fixed) clutter it achieves performance approaching that of the star map technique. An attractive feature of this method is that the normalizer does not use additional information and may thus be applied to a wider range of problems.

Due to the enormous storage requirement associated with a bank of precomputed matched filters, it is preferable (and in the present application easy) to analytically compute the Fourier volume filter in real time. By recognizing that the peak output SNR will occur in a known plane, one may reduce the three-dimensional inverse Fourier transform to a two-dimensional transform, thus saving considerable computation.

The final result is a theory that quantitatively describes many of the features found in typical space surveillance data sets. From this theory P_d and P_{fa} predictions can be generated for various cases, and the relationship between camera noise, object brightness, and observation time required for detection can be estimated. A benchmark of performance is provided for comparison with various computationally efficient implementations. This work also highlights the conflict between optimizing detector configuration for maximum unprocessed SNR versus optimizing for the estimation of a feature. For example, it is desirable to have large pixels relative to the PSF to maximize target signal in relation to CCD readout noise. On the other hand, the signal processing dictates pixels much smaller than the PSF to reduce position dependence in the matched filter.

5. FUTURE WORK

Future work should include an analysis of a statistically significant number of visible- and IR-band image sets, which would allow complete end-to-end description and verification of processing performance in terms of P_{fa} and P_d. Using data sets collected in the laboratory with a scene generator could help clarify the distinction between Poisson photon statistics and jitter effects. A discussion of the number and orientation of three-dimensional filters followed by an automatic search routine would be a required step to develop a deployed system. When using a number of filters there is some leakage of signal between those adjacent, resulting in detection of a single object at several nearby velocities. An analysis of this phenomenon and development of suitable postdetection algorithms to identify the single proper velocity are needed.

Following clutter suppression and signal enhancement, the next step in the signal processing chain is the clustering of detection points into target streaks and the subsequent estimation of target location. One unresolved question is the effect of the signal enhancement processing on position estimation, and specifically, how will the use of the two-dimensional SNR peak rather than the full three-dimensional result affect position estimation?

Another useful direction would be to determine the optimal approximation to matched filter processing for a specified level of available computing power. Thus if matched filter processing is recognized as optimal but only 80% of the required processing power is available, can an optimal use of that processing power be determined? At least two approaches suggest themselves. One is to retain the matched filter and reduce the number of velocity filters; the other is to design suboptimal algorithms that in some limit approach the matched filter.

Using the theory developed herein one could discuss a number of interesting situations, one of which is the minimum resolvable separation for two objects on a common trajectory. A detector implemented on a spacecraft is subject to gamma ray bombardment, leading to many high intensity, single pixel events. Thus appropriate gamma circumvention techniques should be developed. Another area of interest is to estimate the minimum detectable size for low earth orbit debris, utilizing the present image acquisition hardware and estimates of debris reflectance. Finally, much of this work should be directly applicable to look-down surveillance applications with radically different background clutter characteristics.

APPENDIX

DISCRETE FOURIER TRANSFORM REPRESENTATION

A description of the Fourier volume may be developed using a discrete representation and a discrete Fourier transform. The physical intensity distribution incident on the focal plane is continuous in both space and time. A target having a nonvarying spatial distribution but allowed to vary in overall intensity and translate with velocity v may be written

$$\begin{aligned} I(\bar{x},t) &= f(\bar{x}-\bar{x}_s(t))\bullet g(t) \\ &= f(\bar{x}-\bar{x}_o-\bar{v}_s t)\bullet g(t) \quad . \end{aligned} \tag{A-1}$$

The $g(t)$ term allows intensity variation as a function of time, such as target signature. For this work $g(t) = 1$. The starting position at time $t = 0$ is given by x_o. The function $f()$, representing the translating target intensity distribution, may be represented by any number of functions. For example,

$$f(\bar{x}-\bar{x}_o-\bar{v}_s t)=\begin{cases} I_o e^{-(\bar{x}-\bar{x}_o-\bar{v}_s t)^2/2\sigma^2} \\ \text{or} \\ I_o \delta(\bar{x}-\bar{x}_o-\bar{v}_s t) \end{cases} .$$

Next a detector is assumed to have N_x by N_y pixels, each of width $w_x \times w_y$. It is further assumed that N_t frames of data will be collected, each having an integration time T. The observed pixels will then have values

$$g(i,j,k)= \int_{-\infty}^{+\infty}\iiint f(\bar{x}-\bar{x}_o-\bar{v}_s)\ \text{rect}\left[\frac{t-(k+\frac{1}{2})T}{T}\right]\text{rect}\left[\frac{x-(i+\frac{1}{2})w_x}{w_x}\right]$$

$$\text{rect}\left[\frac{y-(i+\frac{1}{2})w_y}{w_y}\right]\,dxdydt \tag{A-2}$$

$$\begin{aligned} i &= 0, \ldots N_x-1 \quad (x \text{ pixel index}) \\ j &= 0, \ldots N_y-1 \quad (y \text{ pixel index}) \\ k &= 0, \ldots N_t-1 \quad (\text{frame index}) \quad , \end{aligned}$$

which it would be desirable to reduce to the form $g(i,j,k) = g(i - kv'_x - x_o/w_x,\ j - kv'_y - y_o/w_y)$ for reasons discussed below.

If the δ-function representation is used, then after substituting $v = v'\ w/T$ and $z = t/T$, the result is

$$g(i,j,k) = I_o T \int_{-\infty}^{+\infty} \mathrm{rect}\left[z - \left(k + \frac{1}{2}\right)\right] \mathrm{rect}\left[\bar{v}' z + \frac{\bar{x}_o}{\varphi} - \left(i + \frac{1}{2}\right)\right] dz \quad . \qquad (A-3)$$

The discrete Fourier transform [15] is

$$G(m,n,p) = \frac{I_o}{\sqrt{N_x N_y N_t}} \sum_{i=0}^{N_x-1} \sum_{j=0}^{N_y-1} \sum_{k=0}^{N_t-1} g(i,j,k) e^{-i\frac{2\pi mi}{N_x}} e^{-i\frac{2\pi nj}{N_y}} e^{-i\frac{2\pi pk}{N_t}} \quad . \qquad (A-4)$$

To form a matched filter, the unknown, initial position information must be separated from the rest of the expression [recall that in the continuous case, Equation (10), this process amounted to a simple phase factor]. Thus not only do Equations (A-3) and (A-4) not lead to closed form solutions, they are fundamentally unsuitable because of this nonseparable property. A true matched filter has to test not only every velocity, but every starting position for every velocity.

When instead of the δ function a Gaussian distribution is used, the result is no better. In two dimensions the problem is indeed tractable, leading to

$$g(i,k) = \sqrt{2\pi}\ \sigma I_o \int_{kT}^{(k+1)T} [\mathrm{erf}(((i+1)w - x_o - vt)/\sigma) - \mathrm{erf}((iw - x_o - vt)/\sigma)]dt \quad ,$$

which may be evaluated using

$$\int \mathrm{erf}(a+bx)dx = \frac{1}{b}\left[(a+bx)\mathrm{erf}(a+bx) + \frac{1}{\sqrt{2\pi}} e^{-\frac{1}{2}(a+bx)^2}\right]$$

to eventually yield a messy combination of error functions and Gaussians that are in the form $g(i - v'k - x_o/w)$. Unfortunately, in three dimensions the problem has proven intractable. This formulation nevertheless can be used to generate test data sets as long as the target velocity is confined parallel to one axis of the pixel array. The use of the Gaussian PSF provides a much closer representation of real data sets than the simple δ-function form.

In light of the foregoing limitations, the model of the satellite is used with the following approximation:

$$I(\bar{x},t) = I_o g(\bar{x} - \bar{v}_s t - \bar{x}_o) \quad . \qquad (A-5)$$

The discrete Fourier transform is

$$G(m,n,p)=\frac{I_o}{\sqrt{N_x N_y N_t}}\sum_{i=0}^{N_x-1}\sum_{j=0}^{N_y-1}\sum_{k=0}^{N_t-1} g(\bar{x}-\bar{v}_s t-\bar{x}_o)e^{-i\frac{2\pi mi}{N_x}}e^{-i\frac{2\pi nj}{N_y}}e^{-i\frac{2\pi pk}{N_t}} \quad .$$

In this case $dk_x = 2\pi/N_x$, $dk_y = 2\pi/N_y$, $d\omega = 2\pi/N_t$ and $k_x = mdk_x$, $k_y = ndk_y$, $\omega = pd\omega$. Several new variables are introduced: $z_1 = i - x_o/w - kv'_x$ and $z_2 = j - y_o/w - kv'_y$, and $i_o = x_o/w_x$, $j_o = y_o/w_y$, yielding:

$$\begin{aligned} G(m,n,p)=&\frac{I_o}{\sqrt{N_x N_y N_t}}e^{-i\frac{2\pi mi_o}{N_x}}e^{-i\frac{2\pi nj_o}{N_y}} \\ &\times\left[\sum_{z_1=-x_o/w-kv'_x}^{(N_x-1)-x_o/w-kv'_x}\sum_{z_2=-y_o/w-kv'_y}^{(N_y-1)-y_o/w-kv'_y} g(z_1,z_2)e^{-i\frac{2\pi z_1 m}{N_x}}e^{-i\frac{2\pi z_2 n}{N_y}}\right] \\ &\times\left[\sum_{k=0}^{N_t-1} e^{-i2\pi\left(\frac{p}{N_t}+\frac{mv_x}{N_x}+\frac{nv_y}{N_y}\right)k}\right] \quad . \end{aligned} \qquad (A-6)$$

If $g(z_1,z_2)$ is sufficiently well behaved that periodic boundary conditions can be invoked, the double summation reduces to the Fourier transform of the single frame target signature. Thus,

$$G(m,n,p)=\frac{I_o}{\sqrt{N_x N_y N_t}}e^{-i\frac{2\pi mi_o}{N_x}}e^{-i\frac{2\pi nj_o}{N_y}}G(m,n)\left[\frac{\sin(\pi\gamma N_t)}{\sin(\pi\gamma)}e^{-i\pi(N_t-1)\gamma}\right] \quad , \qquad (A-7)$$

where $= \gamma = \left[\frac{p}{N_t}+\frac{mv_x}{N_x}+\frac{nv_y}{N_y}\right]$.

This is easily seen to be the discrete equivalent of Equation (10). The signal is maximized in the plane

$$p = N_t\left[\frac{mv_x}{N_x}+\frac{nv_y}{N_y}\right] \quad . \qquad (A-8)$$

The matched filter is then the complex conjugate of $G(m,n,p)$, with $i_o = j_o = 0$:

$$H(m,n,p) = \frac{I_o}{\sqrt{N_x N_y N_t}}\, G(m,n) \left[\frac{\sin(\pi\gamma N_t)}{\sin(\pi\gamma)}\, e^{-i\pi(N_t-1)\gamma} \right] \qquad (A-9)$$

$$= \frac{I_o}{\sqrt{N_x N_y N_t}}\, G(m,n)\, \frac{\sin(\pi\gamma N_t)}{\sin(\pi\gamma)} \left\{ \cos[\pi(N_t-1)\gamma] + i\sin[\pi(N_t-1)\gamma] \right\} \quad .$$

Unfortunately, periodic boundary conditions cannot normally be invoked because the signature varies from frame to frame. It is important to note that this is not an intrinsic signature $g(z_1,z_2)$ but one that is induced due to the integration effects of the finite pixels. If the (Gaussian) PSF is larger than a single pixel, the signature will not vary from frame to frame; however, in the case where σ is on the order of a pixel size, significant velocity-dependent effects arise. The worst case is a narrow PSF and low velocities, on the order of 1.5 pixels per frame.

SYMBOLS

P_d	probability of detection
P_{fa}	probability of false alarm
N_x, N_y, N_t	number of pixels in x,y direction and number of frames
$\eta(t)$, $N(\omega)$	Fourier transform pair representing noise
$s(t)$, $S(\omega)$	Fourier transform pair representing signal
$R(\tau)$	autocorrelation function (of noise)
x_o, t_o	object starting position
k, ω	spatial and temporal frequency components
$I(x,t)$	focal plane intensity distribution
I_ξ, I_η, I_s	star, noise, and signal contribution to focal plane intensity distribution
v_s, V_s	pixel and total data volume
p_x, p_y, p_t	pixel dimensions
L_x, L_y, T	total data volume dimensions
σ	Gaussian point spread distribution parameter
v	target velocity
$v_f = v'$	target velocity in pixels/frame
A_s	target Gaussian peak intensity
E_s	total signal energy per frame
P	signal power
e_s	average signal energy per pixel
ρ_p	observed noise standard deviation per pixel
η	background average value
Ω	total number of pixels in a streak
E_η	noise energy
v_F, V_F	Fourier volume per pixel, total Fourier volume
$G(k,\omega)$	Fourier transform of signal

B_s	$\sigma^2 A_s$
i,j,k	indices referring to space-time data
m,n,p	indices referring to Fourier volume data
α	threshold parameter (in units of standard deviations)
SNR_s,SNR_f	signal-to-noise ratio of original (s) and filtered (f) data
λ	$\rho_p \sqrt{\Omega}$
CNR	clutter-to-noise ratio (SNR of stars)
γ	$\gamma = 0$ defines Fourier plane of maximum signal

REFERENCES

1. C.E. Cook and M. Bernfeld, *Radar Signals*, New York: Academic Press (1967), pp 5–24.
2. W.K. Pratt, *Digital Image Processing*, New York: John Wiley & Sons (1978), pp 551–561.
3. I.S. Reed, R.M. Gagliardi, and H.M. Shao, "Application of three-dimensional filtering to moving target detection," *IEEE Trans. Aerosp. Electron. Syst.*, **AES-19**, pp. 898–904 (1983).
4. B. Porat and B. Friedlander, "A frequency domain approach to multiframe detection and estimation of dim targets," *Proc. IEEE Int. Conf. Acoust. Speech Signal Processing*, 591 – 594 (1987).
5. I.S. Reed, R.M. Gagliardi, and L. Stotts, "Optical moving target detection with 3-D matched filtering," *IEEE Trans. Aerosp. Electron. Syst.*, **AES-24**, 327–335 (1988).
6. D.A. Scribner, M.S. Longmire, and M.R. Kruer, *Analytic modeling of staring infrared systems with multidimensional matched filters, Proc. SPIE,* **890**, 81–91 (1988).
7. K.R. Castleman, *Digital Image Processing*, Englewood Cliffs, N.J.: Prentice-Hall (1979), pp. 190–225.
8. L.W. Wainstein, and V.D. Zubakov, *Extraction of Signals from Noise*, Englewood Cliffs, N.J.: Prentice-Hall (1962).
9. S.C. Pohlig, "Maximum Likelihood Detection of Electro-optic Moving Targets," Lexington, Mass.: Lincoln Laboratory, Technical Rep. 940 (16 January 1992).
10. G. Arfken, *Mathematical Methods for Physicists*, New York: Academic Press, (1970) pp. 249, 467–469.
11. W.H. Press et al., *Numerical Recipes in C*, New York: Cambridge University Press (1988), pp. 398–470.
12. N.H. Wells, C.S. Burrus, G.E. Desobry, and A.L. Boyer, "Three-dimensional Fourier convolution with an array processor," *Computers in Physics*, 507–513 (1990).
13. J.W. Goodman, *Introduction to Fourier Optics*, New York: McGraw-Hill (1968) pp. 21–25.
14. A.D. Stocker and P. Jensen, "Algorithms and architectures for implementing large velocity filter banks," *Proc. SPIE,* **1481** (1991).
15. E.O. Brigham, *The Fast Fourier Transform*, Englewood Cliffs, N.J.: Prentice-Hall (1974), pp. 91–99.

REPORT DOCUMENTATION PAGE

Form Approved
OMB No. 0704-0188

1. AGENCY USE ONLY (*Leave blank*)	2. REPORT DATE	3. REPORT TYPE AND DATES COVERED
	30 September 1992	Technical Report

4. TITLE AND SUBTITLE

Optimal Three-Dimensional Matched Filter Processing for Detection of Point-Like Moving Objects in Clutter

5. FUNDING NUMBERS

C — F19628-90-C-0002
PE — 63220C
PR — 287

6. AUTHOR(S)

John N. Sanders

7. PERFORMING ORGANIZATION NAME(S) AND ADDRESS(ES)

Lincoln Laboratory, MIT
P.O. Box 73
Lexington, MA 02173-9108

8. PERFORMING ORGANIZATION REPORT NUMBER

TR-946

9. SPONSORING/MONITORING AGENCY NAME(S) AND ADDRESS(ES)

Strategic Defense Initiative Organization
OSD/SDIO/SN
The Pentagon
Washington, DC 20301-7100

10. SPONSORING/MONITORING AGENCY REPORT NUMBER

ESD-TR-91-244

11. SUPPLEMENTARY NOTES

None

12a. DISTRIBUTION/AVAILABILITY STATEMENT

Approved for public release; distribution is unlimited.

12b. DISTRIBUTION CODE

13. ABSTRACT (*Maximum 200 words*)

A simple model of a time sequence of star images containing a moving point object (satellite) is developed. Optimal signal enhancement and detection processing theory is applied to this model and a three-dimensional Fourier matched filter implementation is derived to compute clutter-to-noise ratio (CNR) suppression, signal-to-noise ratio (SNR) enhancement, and probability of detection (P_d) and false alarm (P_{fa}) rate estimates as a function of input single pixel SNR. Using this theory allows one to compute the Fourier domain matched filters directly, thereby eliminating the enormous storage cost associated with large banks of three-dimensional matched filters. The model and theory are tested using computer-generated simulated data sets having known noise and clutter characteristics. The theory is then applied to real data sets collected using a Lincoln Laboratory CCD camera. Initial results indicate good agreement with matched filter theory. Detection of objects with an initial single pixel SNR ≈1 is demonstrated.

14. SUBJECT TERMS

matched filter; clutter suppression; detection; Fourier transform; electrooptic; surveillance; moving target

15. NUMBER OF PAGES
62

16. PRICE CODE

17. SECURITY CLASSIFICATION OF REPORT	18. SECURITY CLASSIFICATION OF THIS PAGE	19. SECURITY CLASSIFICATION OF ABSTRACT	20. LIMITATION OF ABSTRACT
Unclassified	Unclassified	Unclassified	SAR